Numerical studies of advanced combustion concepts in hydrogen and methanol compression ignition engines

Treacy, Mark

2024

Document Version:
Publisher's PDF, also known as Version of record

Numerical studies of advanced combustion concepts in hydrogen and methanol compression ignition engines

MARK TREACY
DEPARTMENT OF ENERGY SCIENCES | FACULTY OF ENGINEERING | LUND UNIVERSITY

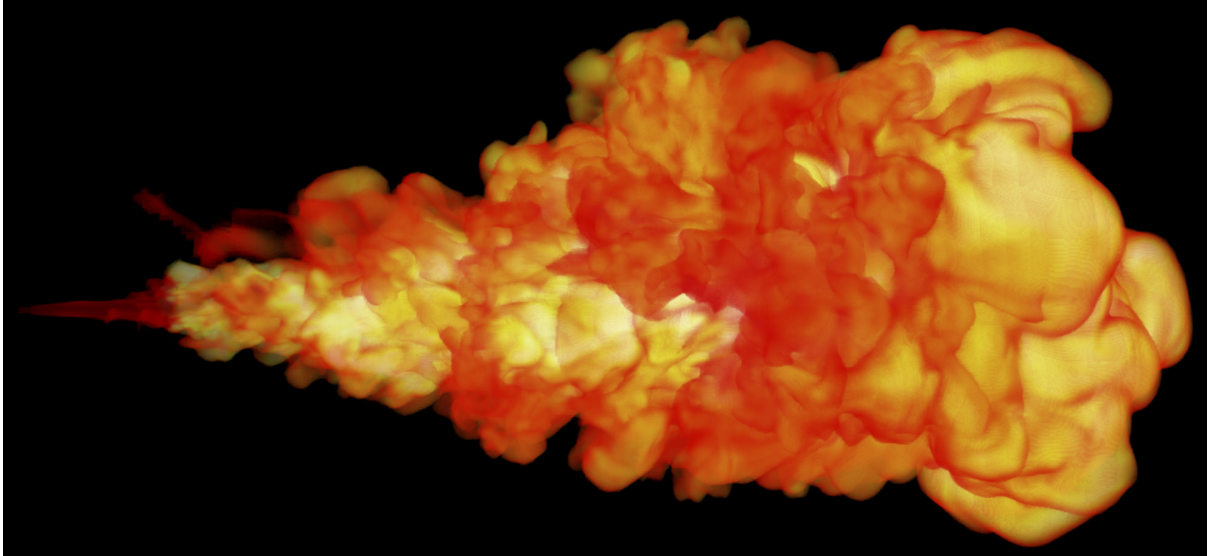

Printed by Media-Tryck, Lund 2024 NORDIC SWAN ECOLABEL 3041 0903

Faculty of Engineering
Department of Energy Sciences

ISBN 978-91-7895-998-3

Numerical studies of advanced combustion concepts in hydrogen and methanol compression ignition engines

Numerical studies of advanced combustion concepts in hydrogen and methanol compression ignition engines

by Mark Treacy

LUND
UNIVERSITY

Thesis for the degree of Doctor of Philosophy
Thesis advisors: Prof. Xue-Song Bai, Assoc. Prof. Hesameddin Fatehi
Faculty opponent: Prof. Hongming Xu

To be presented, with the permission of the Faculty of Engineering of Lund University, for public criticism in lecture room M:B, at M-Building on Friday, the 31st of May 2024 at 10:15.

Organization
LUND UNIVERSITY

Department of Energy Sciences
Box 118
SE–221 00 LUND
Sweden

Document name
DOCTORAL THESIS

Date of disputation
2024-05-31

Sponsoring organization

Author(s)
Mark Treacy

Title and subtitle
Numerical studies of advanced combustion concepts in hydrogen and methanol compression ignition engines

Abstract
The effects of climate change have led to increasing concern regarding global emissions, especially carbon dioxide (CO_2) emissions. A significant contributor to these emissions is the combustion of fossil fuels in internal combustion engines (ICEs). This combustion process is also responsible for other harmful emissions such as carbon monoxide (CO), soot, and nitrogen oxides (NO_x). Although significant improvements have to be made to ICEs, making them produce less emissions and high efficiency, it can be very difficult to remove them entirely using fossil fuels. Due to this, interest in electrification has grown rapidly in recent years. However, electrification of heavy-duty vehicles may not be suitable because of the high energy demand, which would require a larger amount of batteries and, therefore, less space for payload.

An alternative to electrification is ICEs, which use alternative fuels that can achieve cleaner combustion than fossil fuels. Among the potential fuels that could replace fossil fuels are methanol, an alcohol-based fuel, and hydrogen, a carbon-free fuel. However, research and development on the engines operating with these fuels are needed to incorporate them into the engines. In particular, advanced engine concepts, such as low-temperature combustion (LTC), single-fuel stratification, and dual-fuel stratification have shown great potential for methanol and hydrogen fuel operation. To this end, an understanding of the combustion behaviour of both of these fuels under these advanced engine concepts is desirable. This thesis used computational fluid dynamics (CFD) to investigate the combustion and emission process of these fuels in heavy-duty compression ignition engines, under LTC conditions in single-fuel and dual-fuel engine conditions. For the methanol LTC engine studies, this thesis contributed to the understanding of the impact of fuel injection timing on engine performance and emissions. The interaction of methanol spray with the engine piston bowl is critical for the forming of optimal mixture stratification in the engine to achieve simultaneous high efficiency and low emissions of NO_x, CO, and unburned fuels. For the hydrogen single-fuel and dual-fuel engines, this thesis contributed to the development of zero-carbon hydrogen engine operation.

A challenge with hydrogen in CI engines is the controlled combustion. To achieve this, a more reactive fuel such as diesel can be used to ignite the hydrogen. The first hydrogen work in this thesis investigates this dual-fuel strategy where diesel is injected prior to the hydrogen injection. In this work, three SOIs are investigated at two different rail pressures. The highest efficiency of 54.9% is achieved at the earliest injection with high rail pressure. The rail pressure does not significantly impact the efficiency but rather the SOI timing, which results in higher exhaust losses for later injection cases. A similar trend for NO_x and efficiency was observed. In the second hydrogen work, single-fuel stratification is investigated by replacing the diesel pilot with a hydrogen pilot. The purpose is to create a mixture formation that will provide a sufficient ignition source for the main hydrogen injection. This was done by a large test matrix where the dwell time and pilot energy share were adjusted. The main injection SOI was set as the SOI for the highest efficiency case from the dual-fuel simulations. In this study, controlled combustion did not occur without increasing the intake temperature. This section of the work identified a complex relationship between dwell time, pilot energy share, and intake temperature. For given conditions, an efficiency of 52% was achieved but with high NO_x. To increase the potential time for heating, the main injection SOI was shifted close to TDC. This allowed for controlled combustion without the need for an increased intake temperature. Larger pilot energy shares resulted in low NO_x emissions since a larger share of the energy was burned under fuel-lean premixed conditions. Finally, LES was carried out on reacting diesel-hydrogen dual-fuel constant volume case. This study aimed to provide a better understanding of the interaction between diesel and hydrogen by incorporating different dwell times. The study found that hydrogen ignition occurred after some mixing with the n-heptane. With a longer dwell time, the duration of the mixing is longer before mixing.

Key words
Internal combustion engine, methanol, hydrogen, dual-fuel, high-pressure direction injection, large eddy simulation, Reynolds averaged Navier-Stokes simulation, NOx emissions, engine efficiency

Classification system and/or index terms (if any)

Supplementary bibliographical information

Language
English

ISSN and key title

ISBN
978-91-7895-998-3 (print)
978-91-7895-999-0 (pdf)

Recipient's notes

Number of pages
212

Price

Security classification

Numerical studies of advanced combustion concepts in hydrogen and methanol compression ignition engines

by Mark Treacy

LUND
UNIVERSITY

A doctoral thesis at a university in Sweden takes either the form of a single, cohesive research study (monograph) or a summary of research papers (compilation thesis), which the licentiate student has written alone or together with one or several other author(s).

In the latter case the thesis consists of two parts. An introductory text puts the research work into context and summarizes the main points of the papers. Then, the research publications themselves are reproduced, together with a description of the individual contributions of the authors. The research papers may either have been already published or are manuscripts at various stages (in press, submitted, or in draft).

Cover Illustration: Volume rendering of the temperature in the dual-fuel constant volume LES investigation.

Funding information: The methanol part of thesis work was financially supported by the Swedish Energy Agency through the KCFP Research Center. The hydrogen work was sponsored by the Swedish Energy Agency and Scania CV AB.

Faculty of Engineering, Department of Energy Sciences

isbn: 978-91-7895-998-3 (print)
isbn: 978-91-7895-999-0 (pdf)

Printed in Sweden by Media-Tryck, Lund University, Lund 2024

Media-Tryck is a Nordic Swan Ecolabel certified provider of printed material. Read more about our environmental work at www.mediatryck.lu.se

Printed matter 3041 0903

MADE IN SWEDEN

Only you know your true potential

Contents

List of publications

This thesis is based on the following publications, referred to by their Roman numerals:

I **Comparison of efficiency and emission characteristics in a direct-injection compression ignition engine fuelled with iso-octane and methanol under low temperature combustion conditions**
Leilei Xu, **Mark Treacy**, Yan Zhang, Amir Aziz, Martin Tuner, Xue-Song Bai
Applied Energy, 2022, 312, 118714

II **Performance of a methanol fuelled direct-injection compression ignition heavy-duty engine under low temperature combustion conditions**
Mark Treacy, Leilei Xu, Hesameddin Fatehi, Xue-Song Bai
12th Mediterranean Combustion Symposium, 2023, Luxor, Egypt

III **Performance and emissions of a novel high-pressure direct injection dual-fuel engine**
Mark Treacy, Ahmad Hadadpour, Xue-Song Bai, Hesameddin Fatehi
Under review in Fuel

IV **A Computational Fluid Dynamics Study of Advanced Injection Strategies for Compression Ignition Hydrogen Engines**
Mark Treacy, Ahmad Hadadpour, Xue-Song Bai, Hesameddin Fatehi
Manuscript to be submitted

V **Large eddy simulation of diesel-hydrogen dual-fuel flames**
Mark Treacy, Xue-Song Bai, Hesameddin Fatehi
Manuscript to be submitted

Publications not included in this thesis:

I **Effect of piston bowl geometry and compression ratio on in-cylinder combustion and engine performance in a gasoline direct-injection compression ignition engine under different injection conditions**
Leilei Xu, Xue Song Bai, Yaopeng Li, **Mark Treacy**, Changle Li, Per Tunestål, Martin Tunér, Xingcai Lu
Applied Energy, 2020, 280, 115920

II **A skeletal chemical kinetic mechanism for ammonia/n-heptane combustion**
Leilei Xu, Yachao Chang, **Mark Treacy**, Yuchen Zhou, Ming Jia, Xue Song Bai
Fuel, 2022, 331 Pt. 2, 125830

III **Investigation of hydrogen direct injection jets using a simplified injector geometry**
Mark Treacy, Xue-Song Bai, Hesameddin Fatehi
14th International ERCOFTAC Symposium on Engineering Turbulence Modelling and Measurements, Barcelona, 2023

Abstract

The effects of climate change have led to increasing concern regarding global emissions, especially carbon dioxide (CO_2) emissions. A significant contributor to these emissions is the combustion of fossil fuels in internal combustion engines (ICEs). This combustion process is also responsible for other harmful emissions such as carbon monoxide (CO), soot, and nitrogen oxides (NO_x). Although significant improvements have to be made to ICEs, making them produce less emissions and high efficiency, it can be very difficult to remove them entirely using fossil fuels. Due to this, interest in electrification has grown rapidly in recent years. However, electrification of heavy-duty vehicles may not be suitable because of the high energy demand, which would require a larger amount of batteries and, therefore, less space for payload.

An alternative to electrification is ICEs, which use alternative fuels that can achieve cleaner combustion than fossil fuels. Among the potential fuels that could replace fossil fuels are methanol, an alcohol-based fuel, and hydrogen, a carbon-free fuel. However, research and development on the engines operating with these fuels are needed to incorporate them into the engines. In particular, advanced engine concepts, such as low-temperature combustion (LTC), single-fuel stratification, and dual-fuel stratification have shown great potential for methanol and hydrogen fuel operation. To this end, an understanding of the combustion behaviour of both of these fuels under these advanced engine concepts is desirable. This thesis used computational fluid dynamics (CFD) to investigate the combustion and emission process of these fuels in heavy-duty compression ignition engines, under LTC conditions in single-fuel and dual-fuel engine conditions. For the methanol LTC engine studies, this thesis contributed to the understanding of the impact of fuel injection timing on engine performance and emissions. The interaction of methanol spray with the engine piston bowl is critical for the forming of optimal mixture stratification in the engine to achieve simultaneous high efficiency and low emissions of NO_x, CO, and unburned fuels. For the hydrogen single-fuel and dual-fuel engines, this thesis contributed to the development of zero-carbon hydrogen engine operation.

A challenge with hydrogen in CI engines is the controlled combustion. To achieve this, a more reactive fuel such as diesel can be used to ignite the hydrogen. The first hydrogen work in this thesis investigates this dual-fuel strategy where diesel is injected prior to the hydrogen injection. In this work, three SOIs are investigated at two different rail pressures. The highest efficiency of 54.9% is achieved at the earliest injection with high rail pressure. The rail pressure does not significantly impact the efficiency but rather the SOI timing, which results in higher exhaust losses for later injection cases. A similar trend for NO_x and efficiency was observed. In the second hydrogen work, single-fuel stratification is investigated by replacing the diesel pilot

with a hydrogen pilot. The purpose is to create a mixture formation that will provide a sufficient ignition source for the main hydrogen injection. This was done by a large test matrix where the dwell time and pilot energy share were adjusted. The main injection SOI was set as the SOI for the highest efficiency case from the dual-fuel simulations. In this study, controlled combustion did not occur without increasing the intake temperature. This section of the work identified a complex relationship between dwell time, pilot energy share, and intake temperature. For given conditions, an efficiency of 52% was achieved but with high NO_x. To increase the potential time for heating, the main injection SOI was shifted close to TDC. This allowed for controlled combustion without the need for an increased intake temperature. Larger pilot energy shares resulted in low NO_x emissions since a larger share of the energy was burned under fuel-lean premixed conditions. Finally, LES was carried out on reacting diesel-hydrogen dual-fuel constant volume case. This study aimed to provide a better understanding of the interaction between diesel and hydrogen by incorporating different dwell times. The study found that hydrogen ignition occurred after some mixing with the n-heptane. With a longer dwell time, the duration of the mixing is longer before mixing.

Acknowledgements

The methanol engine work was sponsored by the Swedish Energy Agency through the KCFP Research Center. The hydrogen engine work was sponsored by the Swedish Energy Agency and Scania CV AB within the HYZERO project. The simulations were performed on resources provided by the National Academic Infrastructure for Supercomputing in Sweden (NAISS). The author thanks Convergent Science for providing the CONVERGE licenses and technical support for this work.

Firstly, I would like to thank Professor Xue-Song Bai for giving me the opportunity to work on this interesting topic for my PhD studies. I am grateful for all the discussions and support you have provided me in these past years. I would also like to give thanks to Associate Professor Hesameddin Fatehi who mentored and encouraged me throughout the HYZERO project. I am also grateful for his patience in the many, many discussions that took place during this project. A special thanks goes to Dr. Leilei Xu who showed great patience in helping me expand my knowledge and helping me solve all my OpenFOAM problems that only seemed to happen to me. I am significantly grateful for his patience and friendliness.

I would also like to give a significant thanks to Dr. Ahmad Hadadpour (Hamed), my office mate who was very welcoming and friendly from day 1. Throughout our many discussions, he shared his experiences and knowledge for which I am very grateful. His friendliness and support continued during the HYZERO project. I would like to thank Dr. Mateusz Pucilowski who was also a great office mate, providing me with a foundational knowledge of ICEs and PPC. I am also grateful for his extensive feedback on the HYZERO project. I am grateful to Darius, Eric, Nicola, Dennis and Johan who provided feedback on the HYZERO project in our regular meetings. A special thanks goes to past and present colleagues; Francesco, Morteza, Christian, Michael, Shijie, Yuchen and Sheng. I would also like to thank Dr. Robert Szász for his help with my many technical problems.

I would not have made it this far without the endless love and support from my parents, Helen and Derek. I can always count on them to give sound advice and help me through hardships. I cannot thank them enough for everything they have done for me. My girlfriend Karin has been my biggest supporter during my PhD. She has been there for me on the good and bad days. Her belief in me played a vital role in achieving my PhD. Together, there is no challenge we cannot face.

Popular Science Summary

For decades, people have relied on internal combustion engines (ICEs) for the transportation of people and goods. Throughout the years significant development has been carried out to make ICEs more efficient, and reliable, and reduce emissions. A critical component of ICEs is the combustion of fuels such as gasoline (bensin) or diesel. Combustion of these fuels produces emissions that are harmful to the environment and human health. These emissions include carbon monoxide (CO), carbon dioxide (CO_2), and nitrogen oxides (NO_x). In an effort to minimise these emissions, governing bodies are placing restrictions on the amount of emissions allowed from a combustion engine, which road users and manufacturers must adhere to. However, as time moves on targets for carbon neutrality move closer and restrictions get tighter and tighter. As the regulations get tighter, it becomes more difficult for manufacturers to meet these regulations. Therefore, alternative routes need to be investigated.

A potential alternative is electrification, which has seen a significant rise in popularity in recent years with light vehicles. Electrification of road vehicles meets the emissions regulations because no emissions come directly from the vehicle. However, in many parts of the world electricity is produced from fossil fuel combustion, making the electrification of road vehicles less advantageous. Furthermore, not all vehicles such as trucks and buses are well suited for electrification. The infrastructure and understanding of ICEs are well developed and such a drastic transition towards electrification would make these redundant and require a significant amount of new infrastructure. An alternative should be considered which is changing the fuel used in an ICE. Methanol and hydrogen are among the top potential fuels for ICEs and can be produced renewable, eliminating the dependence on raw fossil materials for fuel.

Methanol has a lower carbon content than conventional fossil fuels, gasoline, and diesel, and would therefore reduce carbon emissions. Hydrogen has zero carbon content and therefore would produce no carbon emissions; however, achieving controlled combustion of methanol and hydrogen can be complex. Both of these can still produce NO_x since the formation of NO_x is dependent on the temperature at which the fuel burns. To avoid this, different techniques can be implemented to reduce the combustion temperature such as injecting the fuel earlier than normal for a diesel engine which is called low-temperature combustion (LTC). This strategy allows more time for the fuel to mix with the air, which leads to a lower concentration of fuel and hence, lower combustion temperature. However, doing so increases the chance of having too low fuel concentration which can lead to misfire (no combustion) but can also negatively impact how the fuel burns, lowering the engine efficiency.

In this work computational fluid dynamics simulation (CFD) is conducted to

investigate methanol in LTC conditions and hydrogen in a compression ignition (CI) engine. A CI engine is used because it maximises the potential efficiency of the engine through high compression ratios, but this means that the fuel is required to self-ignite under high pressure and temperature conditions. Methanol is investigated across different stages of LTC strategies which is dictated by the time at which the fuel is injected. With an early injection, the fuel and air mix very well providing a very low combustion temperature, resulting in ultra low-NO_x emission. This early injection also leads to poor combustion efficiency which leads to an increased level of other emissions like CO. As the fuel is injected later, the emission of CO decreases but then the NO_x emission increases, so a balance needs to be found.

Hydrogen is difficult to implement into a CI engine because it is difficult to ignite under CI conditions without an ignition aid. It behaves a little differently from gasoline or diesel because it is a gaseous fuel. To ignite hydrogen, a very small amount of diesel (easily self-ignited) is injected before the hydrogen injection. The diesel ignites and forms a high-temperature region which ignites the hydrogen. Carbon emissions are still present in the engine but significantly reduced. In this work, key engine operation parameters such as the injection pressure and timing are investigated to develop an understanding of how this engine works which can lead to an optimised engine where efficiency is maximised and emissions are minimised. This thesis also investigates a carbon-free engine using a hydrogen pilot. To do this, the hydrogen injection is divided into two parts, a small injection (pilot injection) up to 20 % of the total injected fuel and then a main injection. The purpose of the pilot injection is to create a mixture that will provide a sufficient temperature increase to ignite the main injection. Optimisation of this injection is required so that the correct level of mixing is achieved to ignite before the main injection. Otherwise, all the fuel can ignite simultaneously, which can damage the engine. A study is carried out where the amount of the pilot and the timing between the pilot and main injection are adjusted to determine the operating window.

This thesis uncovered several important findings impacting the development of methanol and hydrogen engines. First, for methanol LTC engines, the combustion behaviour and emissions of NO_x, CO, unburned fuels, and CO2 under different injection timing conditions are better understood. Experimentally, it has been shown that there is an injection timing window in which the engine is optimal in terms of efficiency and emissions. The relationship between engine performance and mixture conditions is identified. Second, the impact of the diesel injection strategy on the hydrogen CI engine performance is revealed. Third, a zero-carbon emission hydrogen engine concept (HYZERO) is systematically evaluated, showing the promising potential of this concept in the decarbonisation of future ICEs in hard-to-electrify transport sectors.

Chapter 1

Introduction

1.1 Background

In today's world, climate change has become a heavily discussed topic and has had a concerning impact on the planet. One of the significant contributors to climate change is greenhouse gases (GHGs). GHGs contribute to global warming by trapping heat near the Earth's surface, leading to an increase in global surface temperature, with 2023 being the hottest on record [1]. One of the biggest contributors to GHGs is the combustion of fossil fuels, which produces carbon dioxide (CO_2). Therefore, the energy and transportation sectors are the biggest contributors to GHG emissions since they both rely on energy conversion from the combustion of fossil fuels.

The transportation sector plays a critical role in the modern world, both in societal and economic ways, by providing convenient movement for goods and people globally. As the global economy and population grow, so does the demand for the transportation sector. As much as the world relies on the transportation sector to function, the transportation sector relies on dependable powertrains. For decades, cars, trucks, and ships have heavily depended on internal combustion engines (ICE). During their lifespan, ICE technologies have experienced significant advancement, greatly increasing their reliability and efficiency, while reducing harmful emissions. However, conventional ICEs produce energy through the combustion of fossil fuels, which produces harmful emissions such as carbon monoxide (CO), CO_2 and nitrogen oxides (NO_x). Figure 1.1 shows that the transportation sector is one of the biggest contributors of GHGs. These emissions contribute negatively to human health and the environment. With the increasing demand on the transportation sector, a better effort is required to make energy sources more efficient and sustainable.

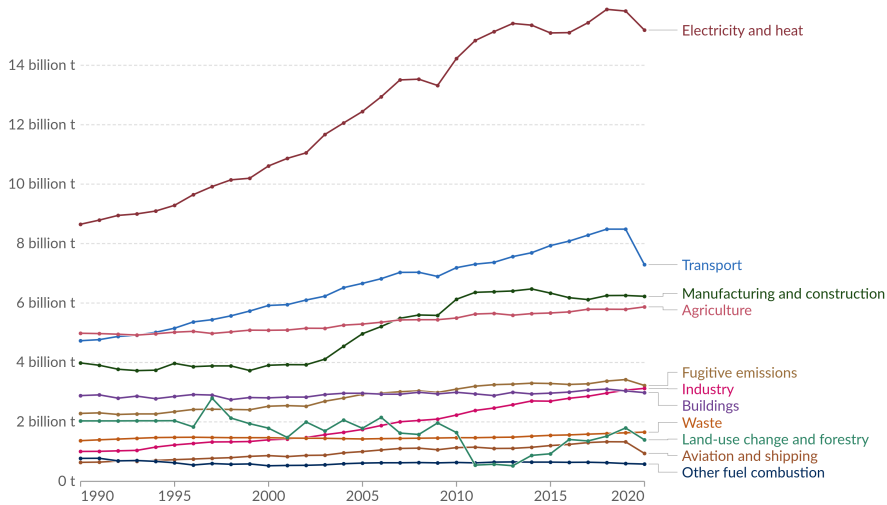

Figure 1.1: The greenhouse gases (tonnes of carbon dioxide equivalents) by sector against the year. [2]

In order to tackle these harmful emissions, governing bodies around the world have introduced restrictions on the emissions allowed by vehicle type. EURO VI [3] is the current regulation standard in Europe targeting the emission of NO_x and particulate matter (PM), with EURO VII [4] expected to be in place by 2035. These strict regulations have led to the rise in electrification of road vehicles where battery electric vehicles (BEVs) contribute to 15% of current vehicle sales [5]. BEVs are able to circumvent these restrictions since they do not produce tailpipe emissions. While the tailpipe emissions are eliminated, emissions are still produced during the mining process for the required raw materials for battery production. Additionally, the source of electricity should be considered since some countries still heavily depend on fossil fuels for energy production. An additional factor to consider for BEV is the durability and lifespan of the batteries which is important considering the rare materials. Electrification of light duty vehicles has been successful with several major car manufacturers producing BEV or hybrid electric vehicles (HEV). However, electrification of heavy-duty vehicles such as trucks and buses is more challenging due to the power demand under high load and the large number of battery cells required. The large batteries required to produce sufficient power can cause problems with packaging the cells and also weight. Since, heavy-duty vehicles depend on maximising the payload, reducing the payload weight for the powertrain is not ideal. An important factor when considering electrification of heavy-duty vehicles is the charging times and charger availability. Heavy-duty vehicles are typically moving for long periods and therefore, short refuelling times are critical. Despite these challenges, electric heavy-duty vehicles are available on the market. However, these vehicles are limited

in range to approximately 300 km depending on the manufacturer [6], and therefore, are restricted to local routes.

While electrification is making progress, the development of the ICEs, particularly for heavy-duty applications, is still ongoing. This development is focused on minimising tailpipe emissions while maximising the efficiency of these power sources. One of the strategies used for minimising tailpipe emissions is the use of aftertreatment systems [7] which reduces emissions by treating the exhaust gases between the exhaust valve and the tailpipe. Aftertreatment systems, such as selective catalytic reduction (SCR) systems [8], capture harmful emissions before they are released from the tailpipe and convert them into less harmful emissions. While aftertreatment systems have been sufficient in meeting emission regulations thus far, stricter regulations impose a greater demand on these systems. These aftertreatment systems are effective in reducing tailpipe emissions; however, this solution does not eliminate emissions and does not prevent the production of these harmful emissions at the source.

To target the source of emissions in the combustion chamber of an ICE, strategies such as low temperature combustion (LTC) [9] can be implemented. LTC strategies aim to reduce NO_x emissions through reduced combustion temperatures since NO_x is primarily formed during high-temperature combustion. LTC strategies aim to reduce the combustion temperature by burning under premixed or partially premixed fuel-lean conditions, realised through early fuel injection. In addition to lean combustion in-cylinder temperatures can be reduced using exhaust gas recirculation (EGR) [10], where the exhaust gas is redirected into the combustion chamber. The inert gases from the exhaust gas absorb heat in the cylinder and therefore, reduce the temperature. While LTC strategies are targeted against NO_x emissions, careful optimisation of injection strategy is required to prevent an increase in other emissions as a result of the lean combustion and also maintain a high efficiency.

The harmful emissions commonly associated with ICEs are produced by the combustion of fossil fuels within the engine. However, ICEs are not limited to the combustion of fossil fuels and many other fuels have been successfully implemented in ICEs. By changing the fuel used in ICEs, to a fuel with a different chemical formulation, the products of combustion also change. Among the suitable candidates for use in ICEs are hydrogen and alcohol-based fuels, such as ethanol and methanol, due to their energy content, octane number and potential for cleaner combustion. Additionally, hydrogen has gained significant attraction as a potential fuel for ICEs, since hydrogen is a zero-carbon fuel [11]. Thus, carbon emissions and particulate matter [12] could be eliminated from the system. Additionally, hydrogen is considered an abundant resource and can be produced renewably [13]. Hydrogen can be implemented not only into ICEs but also fuel cells [14, 15], which can be used for both heavy and light duty vehicles.

Continuous development of ICE is important for a more sustainable and efficient transportation sector. A transition to alternative fuels can lead to more efficient powertrains that produce less emissions than the current fossil fuel engines. Throughout decades of development, a good understanding of fossil fuel combustion in ICE has been formed as well as the systems surrounding the ICE. However, in order to extract the full potential of alternatively fuelled ICEs, a good understanding of the combustion process of these fuels is required, building on existing knowledge. Successful adoption of alternative fuels would lead to minimum alteration of existing infrastructure and lead to cost-effective powertrains.

1.2 Thesis Scope

A deep understanding of the events in the combustion chamber is required to understand the combustion process, emission formation, and overall physics. Typically, experimental works are limited in the measurements that can be made in the combustion chamber, especially without altering the combustion process. Computational fluid dynamics (CFD) can be a useful tool to help understand the in-cylinder events by using numerical modelling to replicate the experiment test points and further expand the available data. This thesis uses numerical methods to simulate the combustion processes of methanol under LTC conditions in heavy-duty ICEs and hydrogen combustion in compression ignition engines. Previous work on methanol under LTC has shown that the injection timing affects the engine performance and emissions. However, the fundamental physics behind this is not clear. In this work, numerical simulations of a methanol LTC engine are employed to investigate the impact of injection timing on the combustion and emission process in the engine.

Literature on hydrogen in ICE applications is focused on spark ignition engines given the challenge of igniting hydrogen. A small number of works investigate hydrogen direct injection compression ignition (DICI) engines; however, there is a significant knowledge gap on how to design a DICI engine based on pure hydrogen. The focus of this thesis is to investigate hydrogen combustion in DICI engines using dual-fuel strategies and pure hydrogen engines based on multiple injection strategies. The study is based on numerical simulations of reference experimental test engines from the literature and collaborators, so that the numerical simulations can be confirmed by experiments. By numerical simulations that provide detailed flow turbulence and thermochemical variables in three-dimensional and temporally resolved, a better understanding of the ignition, fuel interaction and emissions can be provided. Additionally, additional knowledge of the numerical set-up can be provided. Using the simulation set-up and physical engine conditions, this thesis performed a further study investigating strategies to achieve a pure hydrogen DICI engine, namely,

by using pilot/main multiple injection to generate desirable fuel stratification thus achieving optimal ignition of the charge and low NOx emission. This study provides insight into the mixing procedure and ignition of the hydrogen as well as the combustion process of the main injection, shedding light on the future design of DICI engines fuelled only by hydrogen.

Hydrogen high-pressure direct injection (HPDI)s; however, poses a new challenge for both engine experiments and engine simulations. In this thesis, large eddy simulation (LES) is employed to simulate diesel-hydrogen dual-fuel combustion in a constant volume chamber utilising hydrogen HPDI. These simulations are based on experiments carried out under compression ignition conditions. Previous constant volume simulations are focused on non-reacting cases investigating shockwaves in very high-pressure ratio scenarios. LES is used to accurately capture the interaction of the diesel pilot and hydrogen main injection and the following ignition procedure.

1.3 Thesis Objectives

The main objectives can be outlined below, separated by the two fuels investigated:

Methanol:

- Investigation of methanol combustion and pollutant emission in LTC engines. Reynolds Averaged Navier-Stokes (RANS) simulations using detailed chemical kinetic mechanisms are carried out to investigate the impact of the start of injection (SOI) on the engine performance and emissions. The SOI ranges from -100 CAD aTDC to -15 CAD aTDC, covering two LTC regimes, homogeneous charge compression-ignition (HCCI) and partially premixed combustion (PPC).
- Comparison of the methanol LTC engine and gasoline LTC engine performance. A reference gasoline fuel (iso-octane) based LTC engine is also simulated, to understand the impact of the fuel properties and mixture stratification on engine efficiency and pollutant emissions.

Hydrogen:

- Investigation of diesel/hydrogen dual-fuel DICI engine combustion and emissions. Numerical simulations are carried out to replicate the injection process of a pilot diesel and the gaseous hydrogen jet, to understand the interaction

between the two fuels, especially around the time of ignition of the main fuel, and the subsequent main combustion process and NOx emissions.

- Investigation of a pure hydrogen DICI engine concept, in which a multiple injection strategy of hydrogen is studied. Numerical simulations are carried out for a range of pilot-hydrogen injection timings to determine the operating window and impact on the performance of the engine.

1.4 Outline

Chapter 2 will introduce the strategies and concepts discussed in this thesis and present the existing works. This will include an introduction to compression ignition (CI) engines, combustion strategies, and the fuels that will be investigated. Knowledge gaps in the methanol LTC and hydrogen DICI engine combustion will be identified. Chapter 3 will present the governing equations and the models used in the numerical simulations. Chapter 4 outlines the baseline engines and experimental measurements that provided the validation for the simulations, and the equivalent simulation setups. Chapter 5 will present highlight results relevant to the simulations involving methanol, and Chapter 6 will discuss cases investigating hydrogen. More detailed results will be presented in the papers listed in the Appendix. Finally, conclusions and future work will be given in Chapter 7.

Chapter 2

Compression ignition engines and Fuels

2.1 Compression Ignition Engines

There are two different types of internal combustion engines found in road vehicles: spark-ignited (SI) engines and compression ignition (CI) engines. As the name suggests, an SI engine contains a spark plug in the cylinder, providing an ignition source for the fuel-air mixture. In SI engines the fuel is typically injected through port fuel injection (PFI), where the fuel and air mix in the intake manifold before entering the combustion chamber relatively early in the compression cycle. In modern SI engines, direct injection (DI) can be used, providing better control over the injection. By injecting fuel early in the compression stroke, a sufficiently long time is provided for the fuel and air to mix, leading to nearly homogeneous fuel-lean mixtures. Such lean mixtures are beneficial for the reduction of some emissions, such as NO_x. An ignition aid (spark plug) is required in SI engines because of these lean mixtures and also because SI engines typically avail of fuels, such as gasoline, with a high resistance to auto-ignition or high Research Octane Number (RON).

CI engines instead rely on auto-ignition or self-ignition of the fuel-air mixture and therefore, an easily ignitable fuel (low RON), such as diesel is required. The combustion process in CI engines is typically referred to as the conventional diesel cycle (CDC). One of the key differences between the Otto cycle (SI engine) and the CDC, is the compression ratio. To facilitate auto-ignition in CI engines, high temperatures and pressures are provided through high compression ratios. Since the fuel in CI engines must be able to auto-ignite, the risk of premature ignition or knocking is high

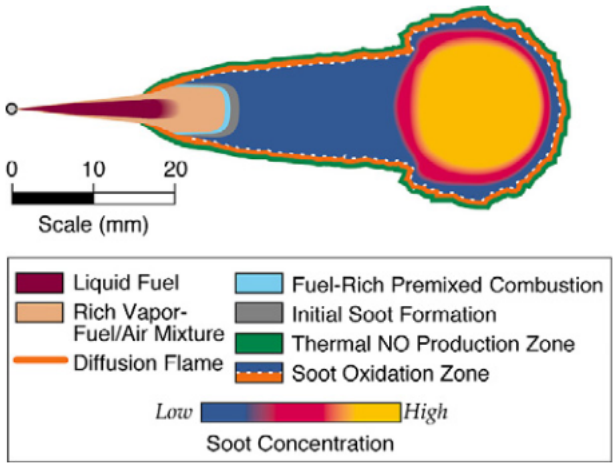

Figure 2.1: The schematic description of CDC from Dec et al. [17, 18].

because of the high compression ratios. To avoid premature ignition, the fuel is injected late in the compression stroke through high-pressure direct injection (HPDI) strategies. Since the fuel is injected close to the top-dead center (TDC), a short time is provided for mixing the air and fuel before ignition should occur. This period between the start of injection (SOI) and the start of combustion is referred to as the ignition delay time (IDT). DI plays a critical role in the CDC because the high-pressure injection leads to atomisation of the liquid or breakup into small droplets [16]. This atomisation process increases the surface area of the fuel, providing faster vaporisation and subsequent mixing with the air.

A widely accepted understanding of the CDC is provided by Dec et al. [17, 18], which is shown in Figure 2.1. It can be seen that premixed and non-premixed combustion play a role in the CDC. The premixed combustion mode is the combustion of a fuel-air mixture that can burn at high speeds, leading to a rapid rate of heat release (RoHR) and a large rise in pressure in the cylinder. The non-premixed mode or diffusion flame burns immediately as the air and fuel enter the reaction zone; hence, the diffusion flame is highlighted at the border around the spray in Figure 2.1. The non-premixed combustion mode, also called mixture-controlled combustion, is limited by the rate at which the reactant (fuel) and oxidizer (air) mix in the reaction zone. Mixture-controlled combustion is the dominant combustion in CI engines; however, premixed combustion is present in the initial phase of heat release. This premixed combustion is present due to the combustion of the fuel-air mixture formed between the start of injection (SOI) and ignition [18].

One of the downsides of CI engines is the emissions of NO_x and soot. The in-cylinder conditions during the combustion of diesel lead to high combustion tem-

peratures, producing high levels of NO_x. Additionally, the short IDT and consequent stratified combustion lead to fuel-rich regions where soot forms, as illustrated in Figure 2.1. A key parameter when investigating the combustion process and emissions is the equivalence ratio, which defines the ratio of air and fuel in a mixture, given by:

$$\Phi = \frac{\frac{m_f}{m_{ox}}}{(\frac{m_f}{m_{ox}})_{st}} \tag{2.1}$$

where m_f and m_ox are the mass of the fuel and oxidiser in the system and $(\frac{m_f}{m_{ox}})_{st}$ is the stoichiometric value of the mixture. The stoichiometric ratio is the ratio where no excess fuel or oxidiser remains following the combustion process and occurs at $\phi = 1$. Therefore, mixtures with $\phi > 1$ are fuel-rich, and $\phi < 1$ is fuel-lean. The air-fuel ratio can also be specified by lambda, which is the inverse of the equivalence ratio.

The equivalence ratio has a significant role in ignition, combustion, and emissions. Excessively fuel-lean or fuel-rich conditions can cause issues with igniting and incomplete combustion. Equivalence ratios around 1 typically burn at high temperatures and, therefore, produce more NO_x than fuel-lean conditions. Additionally, sufficient levels of air are important for the oxidation of soot and CO; however, excessively lean conditions can also prevent oxidation, leading to higher emissions.

Heavy-duty vehicles, such as trucks and buses, rely on CI engines for their efficiency, power output, and reliability. Alternative energy sources, such as electrification and fuel cells, have developed rapidly for light-duty vehicles; however, there are more challenges in implementing these sources in heavy-duty applications. This work focuses on CI engines for heavy-duty applications to maximise the potential efficiency. Additionally, by continuing to use CI engines, major infrastructure changes can be avoided, and the existing understanding and research can remain relevant.

2.1.1 Fuels

A challenge with ICEs is the emissions produced during the in-cylinder combustion processes. Among the emissions produced from the combustion of fossil fuels are soot, CO, CO_2 and NO_x. One of the ways that harmful emissions can be reduced is by changing the fuel that is used in ICEs. Alternative fuels can not only provide cleaner combustion but can also be produced renewably. Existing ICEs have been designed to operate with conventional fossil fuels, such as gasoline and diesel. Therefore, a thorough investigation of alternative fuels is required to determine their suitability. CI engines heavily rely on the chemical properties of the fuel so that auto-ignition can be achieved, providing the in-cylinder conditions. Diesel is highly suitable for CI engines because it has a low RON, an important parameter for CI engines. The opposite

can be said for gasoline, which has a high RON and, therefore, requires a spark for ignition. Future fuels must have similar characteristics to be suitable candidates to replace fossil fuels. Table 2.1 shows a comparison of conventional fossil fuels with methanol and hydrogen.

Table 2.1: Properties of selected fuels related to internal combustion engine use.

Property	Gasoline	Diesel	Methanol	Hydrogen
Chemical formula	mixture	mixture	CH_3OH	H_2
C/H (mass%)	∼6.143	∼6.45	3	0
Density [kg/m^3] (STP)	740	820	790	0.08
Heat of vaporization [kJ/kg]	180∼350	∼256	1100	461
Lower heating value [MJ/kg]	42.9	43.4	20.09	120
Research Octane Number (RON)	100	<20	109	>130
Volumetric Energy Content [MJ/m^3]	31746	38600	15871	8000
Stoichiometric AFR [kg/kg]	15.29	14.32	6.5	34.2
Autoignition temperature [K]	465∼743	527	738	858
Adiabatic Flame Temperature [K]	∼2275	∼2374	2143	2390
Flame speed [m/s]	0.41∼0.58	0.80	0.56	3.25
Flammability limits [Φ]	0.62∼3.89	-	0.55∼4.32	0.1∼7.1
Quenching distance [mm]	∼2.0	-	1.85	0.64

2.1.2 Methanol

Methanol is an alcohol-based fuel with a simple chemical composition compared to conventional fossil fuels. Although this fuel contains carbon, lower carbon emissions can be expected compared to conventional fossil fuel given the lower carbon content [19]. Additionally, by using carbon capture methods to produce methanol, the net emission of carbon can be reduced [20]. The oxygen content and chemical structure of methanol exhibit unique combustion characteristics and reduce the potential for soot formation [21]. Furthermore, the use of methanol in SI and CI engines has shown a reduction of other key emissions such as CO and NO_x [22]. As can be seen from Table 2.1, methanol has a similar density to diesel and gasoline, which allows for easy storage and also has a slightly higher RON than gasoline, making it very suitable for LTC strategies. However, methanol has a lower heating value and volumetric energy content, meaning that a larger injection mass is required per stroke to extract the same amount of energy as diesel or gasoline, which can lead to a higher frequency of refuelling. The flame speed is similar to gasoline, both of which are lower than diesel, which can have a negative influence on combustion efficiency. Additionally, the autoignition temperature is higher than both conventional fossil fuels, which can be beneficial for avoiding pre-mature ignition but also problematic for ignition in CI engines.

Methanol is stored and injected into the combustion chamber as a liquid, and hence, knowledge of liquid DI strategies can be transferred. The injection process occurs at high pressure and introduces several complex physics during the injection, as discussed in the previous section. As the liquid is injected under high pressure, the liquid experiences a breakup into smaller and smaller droplets before vaporising into its gas form. One of the major benefits of methanol for LTC concepts is the decrease of temperature in the mixture due to the vaporisation process [23]. This is indicated by the high latent heat of vaporisation in Table 2.1, which is approximately three times higher for methanol than for diesel. This cooling effect can greatly contribute towards reducing the in-cylinder temperature, which is favourable for the LTC concepts. Another parameter that can be beneficial in LTC concepts is the low stoichiometric AFR, which indicates that fuel-lean conditions can be achieved at a faster rate.

2.1.3 Hydrogen

Hydrogen has recently gained significant attention as fuel for ICEs. One of the major benefits of hydrogen in ICEs is the zero-carbon content [24]. Additionally, the LHV offers a large amount of energy from a small amount of fuel. Hydrogen is considered an abundant resource on earth; however, it must be produced from another substance [25]. Hydrogen production can occur through hydrocarbon reforming, biomass reforming, or water splitting [26]. As with BEVs, it is important to consider the well-to-wheel emissions, and therefore, hydrogen must follow a sustainable production pathway [27]. Carbon emissions can be produced in hydrogen production methods such as hydrocarbon reforming (black/brown hydrogen); however, some production methods using fossil fuels can implement carbon capture [28]. The renewable forms of hydrogen production are biomass reforming and water splitting through electrolysis using renewable energy sources (green hydrogen) [29]. Aside from the carbon content, another benefit to hydrogen is its high energy density based on mass (gravimetric energy density) as seen in figure 2.2; however, it can also be seen that it has a very low volumetric energy density. Therefore, to be stored efficiently, it must be stored in high-pressure fuel tanks. This leads to significant challenges when it comes to storage of the fuel [30]. The construction of some storage tank designs relies on carbon fibre and therefore, should be considered in the life cycle assessment of hydrogen-powered vehicles [31]. Another challenge caused by the low density is implementing HPDI strategies, which will be discussed in Section 2.3.1.

The stoichiometric air-to-fuel ratio (AFR) for hydrogen is higher than that of the other fuels in the table, indicating that hydrogen combustion under lean conditions can be achieved easily. Additionally, the flammability limit in Table 2.1 shows a much wider range for the flammability limits, indicating a wider operating limit than the

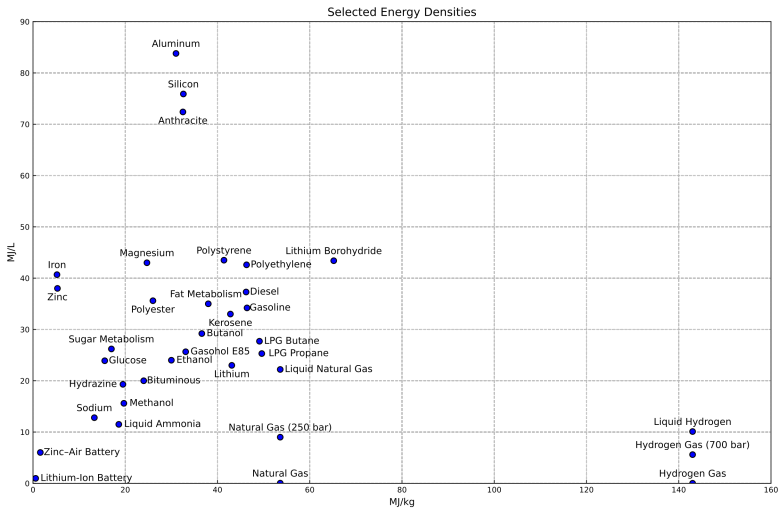

Figure 2.2: The volumetric energy density versus the gravimetric energy density.

other fuels, especially in lean conditions. However, hydrogen is also unique in that it has a high auto-ignition temperature but a low required ignition energy, which can be contradicting. The high auto-ignition temperature provides a challenge for initiating ignition under compression ignition conditions. The low required ignition energy means that only a small amount of energy is required to ignite a hydrogen-air mixture. This makes hydrogen particularly sensitive to remnant ignition sources in the cylinder, such as residual exhaust gases or hot spots. Another consideration for hydrogen is the adiabatic flame temperature and the significantly higher flame speed; while this benefits combustion efficiency, it is detrimental to NO_x formation.

2.2 Low Temperature Combustion Concept

Low-temperature combustion (LTC) [9] is a well-known strategy for reducing the formation of NO_x emissions in the cylinder. Thermal NO_x is produced when nitrogen and oxygen react in high temperatures. Figure 2.3 shows the ranges of temperature and equivalence ratio in which NO_x and soot form, as well as the operating range for CDC, SI, and LTC strategies. From the figure, the operating window for the CDC overlaps into both the soot and NO_x regions. It can be seen from the figure that the target operating window for LTC in the low-temperature regions shows promising features of low NO_x and soot. LTC can be divided into several different strategies such as reactivity-controlled compression ignition (RCCI) [33], homogeneous charge compression ignition (HCCI) [34], and partially premixed combustion (PPC) [35,36].

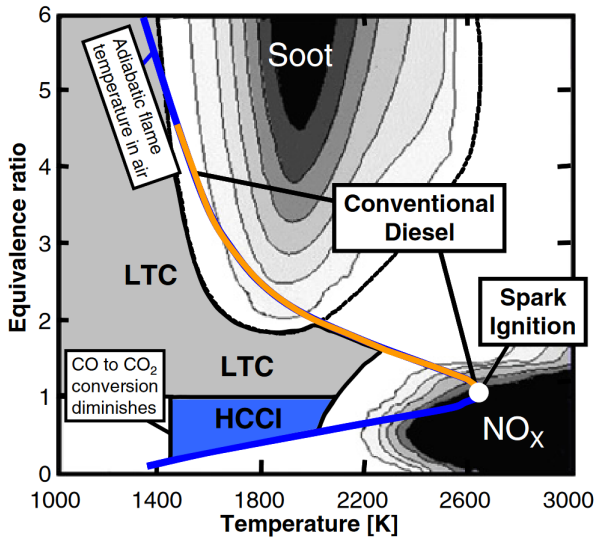

Figure 2.3: The Phi-T diagram showing the regions in which soot and NO_x form and the operating window of CDC, SI, and LTC engines. Reproduced from [32].

RCCI involves separate injections of two fuels: first, a less reactive fuel that has sufficient time to achieve a fuel-lean mixture, before it is ignited by the injection of the more reactive fuel, which ignites the lean mixture of the first fuel. HCCI and PPC rely on a single fuel to achieve lower peak combustion temperatures. Both of these strategies rely on controlling the mixture formation by using the injection timing. As suggested by the name, HCCI aims to produce a homogeneous fuel-lean mixture before ignition. This homogeneous mixture requires a long IDT, and therefore, fuel is injected into the cylinder early in the compression stroke after the intake valve is closed. The fuel-air mixture is locally lean and homogeneous; the ignition process occurs through compression ignition. Given the homogeneity of the mixture, the ignition can occur through multiple ignition kernels throughout the combustion chamber, leading to an intense release of heat. While the lean conditions of HCCI can lead to a reduction in emissions, especially NO_x [37] and soot, it has difficulty maintaining controlled and stable combustion over various loads and can be sensitive to any variations in the cylinder [38]. Additionally, controlling the combustion timing can be difficult since the mixture is ignited using compression ignition rather than a spark plug, and therefore, large cycle-to-cycle variations can be present. PPC strategies implement a more stratified mixture by injecting the fuel later in the compression stroke. There is no general agreement on which strategy should be considered to switch from HCCI to PPC; however, after approximately -60 CAD, aTDC can be considered PPC. As the SOI is retarded towards TDC, the combustion process behaves like the CDC.

High RON fuels are recommended for LTC strategies to avoid premature ignition and allow for large compression ratios. As a result, gasoline under LTC strategies has been heavily researched. Gasoline in PPC strategies has shown promise across various loads [39]. Gasoline PPC shows high indicated efficiencies of approximately 55% with significant reductions in NO_x and soot emissions [40–42]. Sweeping the SOI to cover the HCCI and PPC operating regions shows that the composition stratification has an impact on the emissions [43]. The location of ignition of gasoline fuels under LTC conditions is more sensitive to mixture composition than air temperature [44]. Gasoline in PPC strategies has also shown promising efficiencies and emission levels in light-duty engines [45].

As mentioned earlier, methanol has a significant advantage in LTC strategies since it absorbs a large amount of heat during the evaporation phase of the injection [46]. This cooling effect is beneficial in reducing NO_x emissions by reducing in-cylinder temperatures but also has an impact on the ignition and combustion of methanol. Optical engine studies [47, 48] demonstrate that ignition of methanol can occur at different mixture formations depending on the injection timing. The ignition location occurs in fuel-lean concentrations for early injections but in fuel-rich conditions for late injections. Experiments on methanol PPC in heavy-duty engines show efficiencies up to 53% under high compression ratios [49]. Experiments comparing methanol and a gasoline surrogate, iso-octane, across the HCCI and PPC ranges show lower CO emissions for methanol; however, as the SOI is retarded towards TDC, NO_x emissions see a significant increase [50]. Additionally, both of these fuels achieve different mixture formations in different ranges, affecting engine efficiency.

Numerical studies of methanol PPC show that the special consideration of injection timing should be considered to control the maximum pressure rise rate (MPRR) and RoHR [51]. This is a result of the longer mixing time and the low stoichiometric AFR for methanol, which allows for rapid combustion of the mixture. Other numerical studies demonstrate that increasing the injection pressure leads to an increase in NO_x emissions [51]. This is due to a larger spray plume forming a larger mixture close to stoichiometric conditions, leading to high-temperature combustion. This trend follows the experimental findings [49].

2.3 Hydrogen Combustion

2.3.1 Hydrogen Direct Injection

In ICE applications, hydrogen is in gaseous form, and therefore, its density is significantly lower than that of other liquid fuels. Injecting low-density fuel provides a

new challenge that has not previously been faced. Additionally, the understanding of the injection process and physics of liquid fuels does not directly transfer to gas fuels. Initial studies of hydrogen ICEs involved PFI strategies, given the complexities of DI of low-density fuels. Hydrogen PFI strategies have shown a lower emission of NO_x due to the fuel-lean combustion, which can be achieved due to the wide flammability limits [52]. However, with the PFI strategy, pre-mature combustion is very prone to occur due to the low ignition energy [53, 54]. Additionally, injecting low-density fuel into the intake valve displaces a large portion of air in the intake valve, reducing volumetric efficiency. As a result, research has shifted towards H2 DI strategies [55]. DI strategies can eliminate both pre-mature ignition [56] and low volumetric efficiency [57]. DI can be divided into low (LPDI) and high-pressure direct injection (HPDI), where HPDI is considered above 50 bar.

Gaseous HPDI eliminates some significant issues but also brings new challenges. Injecting a low-density gas leads to very high injection velocities not typically observed in HPDI liquid injection. Such high velocities can result in the formation of expansion waves and introduce new physics. Considering the compressible state of the fuel, an important relationship between the injection pressure and the backpressure or chamber pressure is present. This relationship affects the injection velocity and flow rate and can also see the formation of different types of gas jets. This relationship is characterised by the nozzle pressure ratio (NPR), defined as:

$$NPR = \frac{p_0}{p_\infty} \tag{2.2}$$

where p_0 is the total pressure upstream and p_∞ is the ambient pressure downstream. Three different jet types can form as the NPR changes. A subsonic jet occurs at $1 < p_0/p_\infty < 1.893$, moderately under expanded $2.08 < p_0/p_\infty < 3.8$ and a highly under-expanded jet at $3.84 < p_0/p_\infty$ [58]. Previous work has been carried out investigating the formation of shockwaves and Mach disks under high NPR scenarios using numerical methods [59–63]. However, no previous work has been carried out on reacting cases under high NPRs, so it is unclear how combustion is affected by these very high injection velocities.

Gas HPDI injectors available on the market achieve a much lower rail pressure than their diesel counterparts, operating between approximately 150 bar [64] and 300 bar [65]. The gaseous state hydrogen injection can lead to a variable flow rate based on the injection pressure. Given the compressible state of the gas, the flow can become choked as it passes through the injector nozzle. When the back pressure is equal to or greater than the critical pressure, the flow rate remains constant [66], where the critical pressure is given as:

$$p^* = p_0 \left(\frac{2}{\gamma - 1} \right)^{\frac{\gamma}{\gamma - 1}} \tag{2.3}$$

where p_0 is the upstream pressure and γ is the ratio of specific heats.

An accepted characterisation of direct injection gaseous jets is available from Schlieren experiments [67]. This characterisation separates the jet into a jet core, steady region, and transient vortex region, referred to as the vortex ball [68]. Given the resistance to auto-ignition, significant research has been carried out on the DI of hydrogen in SI engines (DISI). DI strategies have been proven to eliminate backfiring and premature ignition while producing efficiencies above 38.9% even for injection pressures around 80 bar [57]. Other DISI experiments have shown high fuel efficiency and thermal efficiency up to 56% [69]. Numerical studies of DISI strategies [70] show that mixing can be enhanced by increasing the injection pressure of the gas; however, the impact of earlier injection reduces once a uniform mixture has been reached. A study on DISI jet locations found that positioning the jet away from the wall reduced heat losses and achieved high efficiencies [71]. Additionally, this study found that a smaller nozzle hole diameter improved air entrainment, leading to a reduction in NO_x. Another experimental study found that the injector configuration had a larger impact on efficiency in low loads than in high loads [72]. In a separate study [73], an efficiency of 46.9% was achieved with early direct injection in an SI engine. Optical experiments [74] investigate various nozzle geometries with a different number of holes. For thirteen nozzles, the individual jets combine into a single volume. The five-hole option experiences partial jet merging; however, these effects are likely due to the long IDT from the early injection as well as the relatively lower injection pressure of 100 bar. In the numerical simulations [75] of these experiments, the mesh was observed to have a significant impact on the penetration length; however, it did not impact fuel dispersion. Under-prediction of the fuel dispersion was observed; however, the prediction of wall interaction and overall jet evolution showed good agreement with the experiments.

Roy et al. [76] investigated a hydrogen jet in a DISI optical engine. In this study, the injection pressure was found to have an impact on the jet angle, where lower pressure resulted in a wider jet angle; however, the injection pressures were limited to a maximum of 50 bar. Additionally, the chamber density changed the overall structure of the jet. In a constant volume study with higher injection pressures of 53 and 104 bar, Schlieren imaging captured expansion waves that grew large with higher injection pressure [77]. Additionally, it was observed that injection pressure led to a longer penetration length but a higher density led to a lower penetration length.

2.3.2 Diesel-Hydrogen Dual-Fuel DICI Engine

Dual-fuel strategies avail of multiple injections of separate fuels. The purpose of using two fuels is to provide an ignition source by injecting a small amount of reactive fuel,

such as diesel, and a larger amount of less reactive fuel, such as hydrogen. The use of a more reactive is beneficial since it more easily ignites through compression ignition, providing more control over the combustion timing. Such dual-fuel strategies can be implemented in multiple ways: direct interaction between both of the injections (simultaneous injection), pilot injection prior to main injection, and pilot injection after injection. Conventionally, the order of the injection is provided in the name, i.e., diesel-hydrogen, which means the diesel SOI is first.

Dual-fuel strategies are more mature in natural gas applications [78]. This study shows that the overall size of the diesel spray is slightly reduced under dual-fuel methods compared to the single injection operation, and naturally, the injection pressure impacts the time at which the fuels interact. Hydrogen HPDI provides a unique challenge that is shared with natural gas. Studies have been carried out investigating the interaction between a diesel pilot injection and a natural gas main injection. A comprehensive study has been carried out on injector geometry and positioning in a diesel-natural gas dual-fuel engine [79]. Schlieren imaging techniques were used to analyse converging, diverging, and parallel configurations. Naturally, the converging configuration provided high levels of interaction between the fuels. The work highlighted that an overlap of the fuels after ignition can result in the highest performance. This overlap can be achieved by minimising the angle between the converging injectors.

Numerical investigations of the HPDI process for natural gas showed that the nozzle diameter impacts the combustion mode and the efficiency [80]. These studies with natural gas show that the injector configuration (converging, diverging, and parallel) can affect ignition, with ignition occurring under low-temperature ambient conditions using a converging injector [81,82]. However, spray-jet interaction prior to ignition shows a change in the mixture formation of the pilot and can lead to quenching [83]. A study using multiple natural gas injections found that the maximum in-cylinder pressure was lower than a single natural gas injection [84]. For these cases, a diesel pilot is injected prior to the main injection. In multiple injection cases, the main injection is followed by a post-injection. Smaller post-injections combined with longer separation times (time between main- and post-injection) resulted in lower CO emissions due to accelerated oxidation. Alternatively, larger post-injection with shorter separation times led to a reduction in NO_x.

While natural gas HDPI shares some challenges with hydrogen HPDI, recent studies show that these fuels may not behave similarly when it comes to ignition and combustion. In constant volume experiments of diesel-hydrogen strategies, no quenching of the hydrogen was observed [85]. The ignition of the main hydrogen jet occurs after interaction with the pilot flame. For longer dwell times, where the temperature of the pilot region is lower, a longer interaction time is required for the

ignition of the hydrogen jet. Additionally, when the ambient O_2 content is reduced, a higher interaction time is required [86]. Similarly, the lift-off length increases as the O_2 levels are reduced.

Few engine experiments have been carried out using dual-fuel strategies, including hydrogen. One of the studies available shows that at a 50% hydrogen energy share, an indicated efficiency of 47% can be achieved [87]. The emission of NO_x increases as the energy share of hydrogen increases and is also impacted by the level of stratification achieved by the injection timing. Further extending the energy share to 90% achieved an indicated efficiency of 57.2% [88]. However, NO_x emissions were significantly higher than the diesel baseline case. A trade-off was outlined between efficiency and NO_x emissions, where earlier SOI could control NO_x emissions at the cost of efficiency. Numerical simulations of diesel-hydrogen dual-fuel engines showed that high hydrogen energy shares resulted in unstable combustion [89].

2.3.3 Multiple-Injection Hydrogen DICI Engine

Diesel-hydrogen dual fuel engines still emit greenhouse gas CO_2. A goal of a hydrogen-fueled engine is to achieve pure hydrogen DICI operation. Implementing multiple injections can be advantageous by optimising the injections to aid in igniting a fuel that normally requires an ignition aid, such as hydrogen. In order to achieve this, a small fuel injection takes place early in the compression stroke, called a pilot injection. This pilot undergoes mixing with the air in the chamber. Careful consideration of the fuel mass and dwell time is required so that an ignitable mixture is achieved around the time of the main injection. As this pilot injection ignites, the temperature increases to a sufficient level to ignite the main injection. This concept is investigated in this thesis for hydrogen DICI engines.

Single injections of hydrogen in CI engines can lead to uncontrolled combustion or very high MPRR. Multiple injection strategies can be used to achieve different levels of stratification by splitting the main fuel injection into two or more injections [90, 91]. There is a wide number of parameters that need to be taken into account when considering multiple injection strategies, such as the size of the injections and the time between the injections (dwell time). Optimising these injections is critical to enhancing engine performance and reducing emissions. Auto-ignition of hydrogen has been achieved through HCCI strategies with increased intake temperatures of 475 and 675K [92]. In double injection strategies, combustion was observed to be 10 CAD earlier than the single injection. Other works have also achieved HCCI of hydrogen; however, the heat release rate was too high except for overly lean mixtures [93]. Engine experiments of hydrogen only in a CI engine were achieved by increasing the intake temperature to 353 K [94]. A significant improvement in efficiency was observed

compared to the diesel equivalent. Shudo et al. [95] observed that in single injection DI strategies, hydrogen displayed a greater level of diffusion compared to methane. Under split injection conditions, the authors highlight that the spatial distribution of the mixture can be controlled with optimised injector settings.

Constant volume chamber experiments of hydrogen diffusion flames show that the ignition delay is most sensitive to the ambient temperatures rather than other parameters such as injection pressure, nozzle geometry, or chemical composition [96, 97]. In more recent constant volume experiments, a similar trend on ambient conditions is observed [98, 99]. The ignition is observed at a single ignition kernel before spreading around the entire jet, diminishing the liftoff length. In numerical studies of hydrogen ignition in DICI engine applications, hydrogen behaved differently than conventional diesel sprays, achieving better mixing in free-jet mixing [100]. In the double compression-expansion engine (DCEE) concept, ignition of the hydrogen was observed through hydrogen pilot injection, and a BTE calculated from the simulations was measured to be higher than the diesel equivalent [101]. Another numerical work studied various hydrogen combustion strategies, including PFI, DI, and pre-chamber combustion (PCC) strategies [102]; however, no supporting experimental work was provided. In this work, the highest NO_x emissions were measured in the DI dual-fuel case. Meanwhile, the PCC and SI strategies produced ultra-low NO_x.

2.4 Knowledge gap and research questions

Recent experimental research on methanol and iso-octane DICI engines [103], covering HCCI, PPC, and CDC regimes, has shown that CO emissions for methanol engine are generally lower than those for the iso-octane engine. The engine efficiency and emissions for both fuels differ in the different combustion regimes. This is expected to be attributed to the different fuel stratification. There are knowledge gaps regarding the effect of the fuel properties and the injection timing on the engine performance and pollutant emissions, in particular:

- How do the fuel properties affect the engine performance and emissions?
- How does the fuel stratification of methanol and iso-octane evolve under different injection timing conditions?
- Which fuel is more suitable for LTC engines?
- How can the optimal SOI window be extended with high efficiency and low emissions?

These research questions are pursued in Paper I and Paper II, listed in the appendix.

As indicated in the literature, hydrogen DICI engines face several challenges. Most importantly, it is challenging to ensure a controlled ignition of hydrogen due to the high ignition temperature required for hydrogen. Injection of a small amount of pilot fuel, e.g., diesel, can be used to ignite hydrogen; the injection timing of pilot diesel controls the ignition. However, it is uncertain how much pilot diesel should be injected. A higher amount of diesel injection enables reliable ignition, but it can result in high emissions of CO_2 and NO_x. There are knowledge gaps regarding diesel-hydrogen DICI engine combustion:

- How do the fuels interact?
- How does the interaction of these fuels affect the ignition process?
- Which parameters impact engine performance and emissions?
- What are the contributing factors for NO_x production?

This thesis tackles the above questions in Paper III and Paper V, aiming to contribute to improved knowledge of hydrogen DICI dual-fuel engines.

While diesel-hydrogen dual-fuel engines would significantly reduce carbon emissions, the optimal solution would be a carbon-free engine. Therefore, understanding how to ignite hydrogen without needing a spark plug or diesel pilot could be a key step towards the future of hydrogen ICEs. Very little research has been conducted in this direction, and some particular questions exist:

- Can multiple injections of hydrogen be used to generate controlled ignition?
- How does the dwell time between the pilot and main injection affect the ignition and combustion process?
- What is the optimal distribution of the pilot and main injection?
- Can high efficiencies be achieved using pilot/main hydrogen injection?
- Can NO_x be controlled using multiple injections of hydrogen?

These questions will be investigated in Paper IV.

Chapter 3

Numerical Modelling

3.1 Governing Equations

The Navier-Stokes equations are the fundamental equations that are used in computational fluid dynamics (CFD) simulations. The three governing equations represent the conservation of mass, momentum, and energy, and can be written as:

$$\frac{\partial \rho}{\partial t} + \frac{\partial \rho u_j}{\partial x_j} = S_\rho \tag{3.1}$$

$$\frac{\partial \rho u_i}{\partial t} + \frac{\partial \rho u_i u_j}{\partial x_j} = -\frac{\partial p}{\partial x_i} + \frac{\partial \tau_{ij}}{\partial x_j} + S_{u_i} \tag{3.2}$$

$$\frac{\partial \rho h}{\partial t} + \frac{\partial \rho u_j h}{\partial x_j} = \frac{Dp}{Dt} - \frac{\partial J_j^h}{\partial x_j} + S_h \tag{3.3}$$

where u_j is the velocity in the Cartesian coordinate j-direction, P is pressure and h is enthalpy. τ_{ij} is the shear stress in the fluid, which can be written for a Newtonian fluid as:

$$\tau_{ij} = \mu\left(\frac{\partial u_i}{\partial x_j} + \frac{\partial u_j}{\partial x_i} - \frac{2}{3}\frac{\partial u_k}{\partial x_k}\delta_{ik}\right) \tag{3.4}$$

Another important equation to consider in reacting flow is the species transport equation, which is given as:

$$\frac{\partial \rho Y_k}{\partial t} + \frac{\partial \rho u_j Y_k}{\partial x_j} = -\frac{\partial J_j^k}{\partial x_j} + \rho\dot{\omega}_k + S_{Y_k} \tag{3.5}$$

where Y_k is the species mass fraction of species k and $\dot{\omega}_k$ is the reaction rate of species k. J_j^h and J_j^k are the molecular fluxes that can be described by Fick's Law for diffusive mass flux and Fourier's Law for conductive heat flux, written as:

$$J_i^k = -\rho D_k \frac{\partial Y_k}{\partial x_i} \tag{3.6}$$

$$J_i^h = -\rho \alpha \frac{\partial h}{\partial x_i} \tag{3.7}$$

3.2 Equation of state

The equation of state is also a critical equation that is used in the governing equations for compressible flows. For an ideal gas, such as air, the ideal gas law is applicable, which is given as:

$$p = \rho R_u T \sum_{k=1}^{Ns} \frac{Y_k}{W_k} \tag{3.8}$$

where R_u is the universal gas constant and W_k is the molecular weight of species k where N_s is the total number of species. However, the ideal gas law does not apply to hydrogen because hydrogen has a negative Joule-Thompson coefficient. Typically, gases undergo cooling as they experience the expansion process; however, hydrogen is one of two gases that experiences a heating effect. Therefore, a different equation of state is required, which is the Redlich-Kwong equation of state, written as:

$$p = \frac{RT}{v - b} - \frac{a}{v^2 + ubv + wb^2} \tag{3.9}$$

where

$$b = \beta_{rk} v_c \tag{3.10}$$

$$a = \alpha_{rk} \frac{p_c v_c^2}{\sqrt{T_r}} \tag{3.11}$$

where v is the volume, the subscript c indicates the critical conditions, α is the attractive forces between molecules, and β is the volume of the molecules.

3.3 Turbulence

Turbulence can be found everywhere in the day-to-day and is typically characterised as chaotic flow. Turbulent flows consist of turbulent eddies, which are swirling or

rotating fluids. These eddies can be defined by length scale (l), velocity (u), and turnover time (τ). There are three lengths scales considered when simulating turbulent flows: the Integral Scale (l_0), the Taylor Scale (l_λ), and the Kolmogorov Scale (l_η), where the Integral Scale is the largest and the Kolmogorov the smallest. In turbulent flows, eddies begin in the largest scale and as they experience instabilities they break up into smaller scales [104] until they reach a small Reynolds Number, given by:

$$Re = \frac{u_0 l_0}{\nu} \tag{3.12}$$

In numerical simulations, there are three different methods for capturing these turbulent scales. Reynolds Averaged Navier Stokes (RANS) simulations model uses turbulence models, large eddy simulations (LES) resolve the larger scales but rely on models for the smaller scales. Finally, direct numerical simulation (DNS) resolves all of the turbulent scales. However, relying more on resolving the flow required more computational requirements. Therefore, RANS simulations are the most computationally affordable simulations, whereas DNS is the least affordable, such that only small domains can be effectively simulated. This work uses RANS for the simulation of the engine cases and LES for the constant volume study.

3.3.1 Reynolds-Averaged Navier Stokes

In the RANS methods, flow quantities (ϕ) can be divided into an averaged component ($\bar{\phi}$) and a fluctuating component (ϕ') using the Reynolds decomposition written as:

$$\phi = \bar{\phi} + \phi' \tag{3.13}$$

For the following equations, density-weight Favre-filtering is used:

$$\tilde{\phi} = \frac{\bar{\rho\phi}}{\bar{\rho}} \tag{3.14}$$

where ϕ can represent flow variables such as velocity, density, and pressure.

The governing equations given in Section 3.1 under the RANS method become:

$$\frac{\partial \bar{\rho}}{\partial t} + \frac{\partial \bar{\rho}\tilde{u}_j}{\partial x_j} = \bar{S}_\rho \tag{3.15}$$

$$\frac{\partial \bar{\rho}\tilde{u}_i}{\partial t} + \frac{\partial \bar{\rho}\tilde{u}_i\tilde{u}_j}{\partial x_j} = -\frac{\partial \bar{p}}{\partial x_j} + \frac{\partial \bar{\tau}_{ij}}{\partial x_j} - \frac{\partial \bar{\rho}\widetilde{u_i' u_j'}}{\partial x_j} + \bar{S}_{u_i} \tag{3.16}$$

$$\frac{\partial \bar{\rho}\tilde{h}}{\partial t} + \frac{\partial \bar{\rho}\tilde{u}_j\tilde{h}}{\partial x_j} = -\frac{\partial \bar{p}}{\partial x_i} + \frac{\partial}{\partial x_j}\left(\bar{\rho}\tilde{\alpha}\frac{\partial \tilde{h}}{\partial x_j}\right) - \frac{\partial \bar{p}\widetilde{h'u'_j}}{\partial x_j} + \bar{S}_h \tag{3.17}$$

$$\frac{\partial \bar{\rho}\tilde{Y}_k}{\partial t} + \frac{\partial \bar{\rho}\tilde{u}_j\tilde{Y}_k}{\partial x_j} = \frac{\partial}{\partial x_j}\left(\bar{\rho}\tilde{D}\frac{\partial \tilde{Y}_k}{\partial x_j}\right) - \frac{\partial \bar{p}\widetilde{Y'_k u'_j}}{\partial x_j} + \bar{\rho}\tilde{\dot{\omega}}_k + \bar{S}_{Y_k} \tag{3.18}$$

where α is the thermal diffusivity. Using Boussinesq's eddy viscosity assumption [105], the Reynolds stress tensor can be written introducing a turbulent viscosity term:

$$-\bar{\rho}\widetilde{u'_i u'_j} = \mu_t\left(\frac{\partial \tilde{u}_i}{\partial x_j} + \frac{\partial \tilde{u}_j}{\partial x_i} - \frac{2}{3}\frac{\partial \tilde{u}_k}{\partial x_k}\delta_{ij}\right) - \frac{2}{3}\bar{\rho}k\delta_{ij} \tag{3.19}$$

The turbulent viscosity term is obtained through the RANS turbulence models defined by:

$$\mu_t = \bar{\rho}C_\mu\frac{k^2}{\epsilon} \tag{3.20}$$

where k is the turbulent kinetic energy (TKE) and ϵ is the dissipation rate which describes the rate at which the TKE dissipates. C_μ is a coefficient that comes from the model.

3.3.2 Large Eddy Simulation

In the LES method, a filter is required to determine the turbulent scales that are resolved and which are modelled, i.e., subgrid scale (SGS). The filtered variables are written as follows:

$$\tilde{\phi}(x,t) = \int G(x-x')\phi(x',t)dx' \tag{3.21}$$

where G is the filter for LES. The density-weighted Favre-filter (eqn. 3.14) is again used for the LES governing equations as follows:

$$\frac{\partial \bar{\rho}}{\partial t} + \frac{\partial \bar{\rho}\tilde{u}_j}{\partial x_j} = \bar{S}_\rho \tag{3.22}$$

$$\frac{\partial \bar{\rho}\tilde{u}_i}{\partial t} + \frac{\partial}{\partial x_j}\left(\bar{\rho}\tilde{u}_i\tilde{u}_j - \bar{\tau}_{ij} - \tau_{ij}^{sgs}\right) = \bar{S}_{u_i} \tag{3.23}$$

$$\frac{\partial \bar{\rho}\tilde{h}}{\partial t} + \frac{\partial \bar{\rho}\tilde{u}_j\tilde{h}}{\partial x_j} - \frac{\partial}{\partial x_j}\left(\bar{\rho}\tilde{\alpha}\frac{\partial \tilde{h}}{\partial x_j} + \Phi_h^{sgs}\right) = \bar{S}_h + \frac{\partial p}{\partial t} \tag{3.24}$$

$$\frac{\partial \bar{\rho}\tilde{Y_k}}{\partial t} + \frac{\partial \bar{\rho}\tilde{u}_j\tilde{Y_k}}{\partial x_j} - \frac{\partial}{\partial x_j}\left(\bar{\rho}\tilde{D}\frac{\partial \tilde{Y_k}}{\partial x_j} + \Phi_{Y_k}^{sgs}\right) = \bar{S}_{Y_k} + \tilde{\dot{\omega}}_k \tag{3.25}$$

where τ_{ij}^{sgs} is the SGS stress tensor, and Φ_h^{sgs} is the SGS enthalpy flux; both can be modeled using LES eddy viscosity models. A gradient diffusion approach is used for the SGS terms, e.g., for Φ_h^{sgs}:

$$\Phi_h^{sgs} = \bar{\rho}(\tilde{u}_j\tilde{h} - \widetilde{u_j h} = \bar{\rho}D_t\frac{\partial \tilde{h}}{\partial x_j} \tag{3.26}$$

3.4 Combustion Models

The combustion models are responsible for the source term $\tilde{\dot{\omega}}_k$ of species k in the previous equations. In this work, the partially-stirred reactor (PaSR) approach and the SAGE detailed chemical kinetics solver are used.

3.4.1 SAGE detailed chemical kinetics

The SAGE detailed chemical kinetics solver [106] is a combustion solver used in CONVERGE for the hydrogen simulations. This solver behaves like the more well-known, well-stirred reactor (WSR) model. The WSR approach considers the entire mixture within the cell homogeneously mixed. From [107], a multi-step chemical reaction mechanism can be written as:

$$\sum_{j=1}^{J}\nu'_{ji}\chi_j \leftrightarrow \sum_{j=1}^{J}\nu''_{ji}\chi_j \quad \text{for } i = 1, 2, ..., I \tag{3.27}$$

where the stoichiometric coefficients for the reactants and products are given by ν' and ν'', respectively, for species j and reaction i. χ_j is the chemical symbol for species j. The net production rate can be written as:

$$\dot{\omega}_j = \sum_{I}^{i=1}\nu_{ji}q_i \quad \text{for } j = 1, 2, ..., J \tag{3.28}$$

where

$$\nu_{ji} = \nu'_{ji} - \nu'_{ji} \tag{3.29}$$

q_i is the rate-of-progress variable written as:

$$q_i = k_{fi}\prod_{j=1}^{J}[X_j]^{\nu'_{ji}} - k_{ri}\prod_{j=1}^{J}[X_j]^{\nu''_{ji}} \tag{3.30}$$

3.4.2 Partially-Stirred Reactor

The PaSR model [108] is used only for the methanol cases. This approach is similar to the WSR approach; however, instead of assuming a homogeneous mixture, a portion of the cell is considered unmixed. Therefore, only a portion of the cell can undergo combustion, which depends on the reduction factor (κ), given as:

$$\kappa = \frac{\tau_c}{\tau_c + \tau_{mix}} \tag{3.31}$$

where τ_c is the chemical time scale and τ_{mix} is the mixing time scale given as:

$$\tau_{mix} = C_{mix}\sqrt{\frac{\kappa}{\epsilon}\left(\frac{\nu}{\epsilon}\right)^{\frac{1}{2}}} \tag{3.32}$$

C_{mix} is a pre-defined constant that should be calibrated. The source term is then written as:

$$\tilde{\dot{\omega}}_k = \kappa\dot{\omega}_k(\tilde{T}, \tilde{Y_\alpha} \tag{3.33}$$

3.5 Fuel Injection

3.5.1 Liquid Fuel

As a liquid fuel is injected under high pressure into the combustion chamber, it experiences a number of phenomena, such as evaporation and liquid break-up. All of the simulations in this work implement the Lagrangian Particle Tracking (LPT) for the liquid phase. By using LPT, the spray is composed of a number of parcels that contain droplets. The LPT method tracks each of these parcels in the computational domain, where the motion for the parcels is governed by:

$$\frac{d}{dt}\bar{x}_p = \bar{u}_p \tag{3.34}$$

$$\frac{d}{dt}\bar{u}_p = \frac{C_D Re_p}{\tau_p 24}(\bar{u}_g - \bar{u}_p) \tag{3.35}$$

where $\bar{x}_p$ and $\bar{u}_p$ are the position and velocity of the parcel, respectively. $\bar{x}_g$ is the velocity of the gas and τ_p is the characteristic time scale of the parcel. C_D is the coefficient of drag defined as:

$$C_D = \begin{cases} \frac{24}{Re_p}\left(1 + \frac{1}{6}Re_p^{\frac{2}{3}}\right), & Re_p \leq 1000 \\ 0.426, & Re_p > 1000 \end{cases} \tag{3.36}$$

The break-up of these droplets occurs in primary and secondary breakup stages which are modeled by the Kelvin-Helmholtz Rayleigh-Taylor model [109, 110]. In this model, the Kelvin-Helmholtz instabilities cause the primary breakup in the initial length of the spray. In the secondary breakup phase both the Kelvin-Helmholtz and Rayleigh-Taylor instabilities are considered.

3.5.2 Gaseous Fuel

Gaseous fuel injection does not experience the same physics as liquid fuel, and therefore, the same model cannot be implemented for gaseous injection. Similarly, LPT methods are not available within CONVERGE CFD. Instead, the gaseous flow is resolved by specifying a mass flow rate obtained through experimental results. Using the mass flow rate, allowed for control of the injected fuel mass.

3.6 Numerical Solvers

The numerical simulations in this work are carried out using two different numerical solvers. The methanol simulations are carried out using OpenFOAM V7, and the hydrogen simulations are carried out using Converge CFD [111]. OpenFOAM is open-source code providing a wide range of solvers and models, giving it great adaptability for all applications. CONVERGE is a commercial software that has been developed with a large focus on engine and combustion simulations. Converge offers a unique "hands-off" grid generation method, automatically creating structured grids during the simulation.

Chapter 4

Experimental Engines and Computational Cases

4.1 Experimental Measurements

Experimental measurements play a critical role in running CFD simulations by providing validation for the simulation. CFD simulations replicate experimental measurements, and therefore, to determine the accuracy of the simulations, the results between each are compared. The validation stage is critical for determining the accuracy of the set-up and the numerical models as well as the boundary conditions for the case. This thesis relies on two types of experimental work; engine measurements and constant volume chambers.

4.1.1 Engine Measurements

Engine measurements can be divided into optical or metal experiments. Optical experiments produce images of the injection and combustion processes inside the cylinder. Optical experiments use techniques such as particle image velocimetry (PIV), Schlieren and luminosity from chemiluminescence of OH* or CH*. The engine is modified to include windows through which the process is filmed using a high-speed camera. Optical experiments are useful for determining injection penetration length, size of the injection volume, location of ignition and flame growth. Metal engine experiments do not offer any visual data from the cylinder. The cylinder is equipped with pressure transducers, which measure the in-cylinder pressure. From the pressure measurement or pressure trace, the apparent heat release rate (aHRR) of the process

can be calculated using [112]:

$$\frac{dQ}{dt} = \frac{\gamma}{\gamma - 1} P \frac{dV}{dt} + \frac{1}{\gamma - 1} V \frac{dP}{dt} \tag{4.1}$$

where γ is the ratio of specific heats, P is the in-cylinder pressure, and V is the cylinder volume. Since gamma varies throughout the cycle, the gamma from the simulation is used to calculate both the experimental and simulation aHRR. Using the pressure trace and aHRR, the events in the combustion event can be identified. This information can lead to combustion timing, combustion duration, total heat release, and efficiency. Each of these can be used for validation of the simulations. The metal engine experiments are also equipped with measurement systems for taking measurements in the exhaust.

4.1.2 Constant Volume Chamber Measurements

Constant volume (CV) chamber measurements are used to investigate injections and fundamental combustion characteristics. In these cases, a sealed vessel is used alongside imaging techniques to observe the injection and combustion processes. The pressure and temperature in the chamber are similar to those at the point of injection in the engine. This is achieved by completing a pre-burn procedure, where a small amount of fuel is combusted to increase the pressure and temperature.

4.2 Methanol Engine Cases

4.2.1 Case Description

The engine experiments involving methanol were carried out by the engine department at Lund University [50]. The engine used in the experiments was a six-cylinder Scania D13 heavy-duty CI engine with a compression ratio of 17:1. The four-stroke engine was modified so that only one of the six cylinders was operating during the experiments. The in-cylinder pressure was measured with a resolution of 0.2°. The value at which 50% of the chemical energy (CA50) was fixed at 3° CAD aTDC, which was controlled by adjusting the intake temperature. The engine operates with an engine load of 4 bar. In Paper I, methanol and iso-octane, a surrogate of gasoline, were injected in separate measurements at an injection pressure of 800 bar. There is a significant difference in the LHV of these fuels and therefore, in order to inject the same amount of energy the injection duration is different between the fuels. Both of the fuels were injected through a twelve-hole injector with a hole diameter of 230 μm.

To capture the HCCI and PPC operating windows, the SOI was swept from -100° CAD aTDC to -15° CAD aTDC.

4.2.2 Simulation Set-up

The numerical simulations were carried out using OpenFOAM V7 using the RANS framework. A 30° sector of the full engine was used which captures one of the spray plumes. As part of using a sector simulation, the simulation is a closed-cycle simulation that only simulates the time between the intake valve closed (IVC) and the exhaust valve open (EVO), which can be specified as -141 ° CA aTDC and 137° CA aTDC, respectively.

The fuel was injected at an umbrella angle of 120°. The injection profiles for both of the fuels were created using a model for liquid injections [113]. The Lagrangian-Eulerian model was implemented for the modelling of the liquid injections. The KH-RT model was responsible for modelling the breakup. The combustion is modelled using the PaSR model. The same reaction mechanism was used for both fuels, which contains 136 species and 617 reactions [114].

Cartesian cells are used to form the grid of the sector engine. During the simulation, these cells experience compression and expansion as the piston moves, which can lead to poor cell aspect ratios and reduced accuracy. To avoid this a dynamic mesh layer algorithm is used [115]. This algorithm adds and removes cells based on a specified height threshold such that when the minimum height is reached during compression, the cell is removed, and when the maximum height is reached cells are added. Figure 4.1 shows the mesh across various CAD. In addition to the height threshold, the region of the domain where this algorithm function is also specified to be 1 mm above the piston topland (Face Zone in Figure 4.1). Therefore, the cells located below this line and in the piston are not impacted by the algorithm.

4.3 Hydrogen Engine Cases

4.3.1 Case Description

The data for the diesel-hydrogen dual-fuel experiments were provided by Scania CV AB. These experiments were carried out in a Scania D13 heavy-duty CI engine at medium load with a compression ratio of 23:1. During these experiments, all six cylinders were operating with the pressure measured in each cylinder. The engine was operated with an engine load of 16 bar IMEP and a boost pressure of 2.2 bar. The

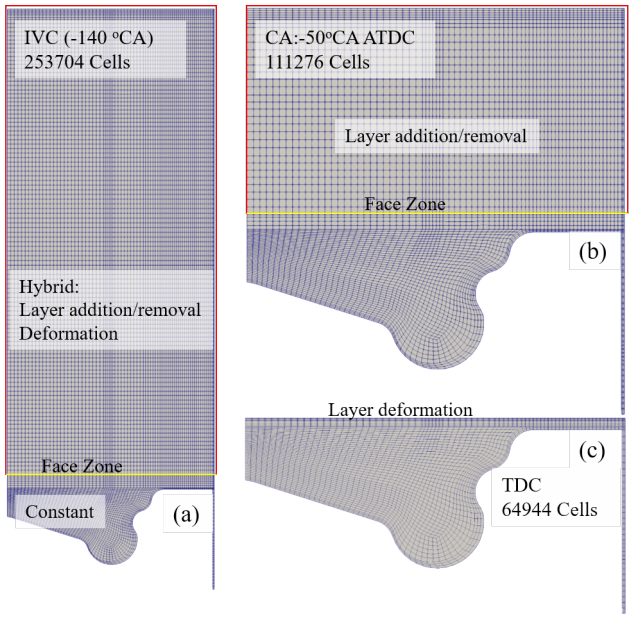

Figure 4.1: The mesh at various crank angle degrees, demonstrating the dynamic mesh algorithm.

pressure trace was averaged over 300 cycles and then averaged over each cylinder. The swirl ratio for these cases is 1.5.

The liquid diesel and gaseous hydrogen were injected through the same injector but through a different set of holes. The injector has a total of eighteen holes, nine for the diesel injection and nine for the hydrogen injection. The diesel holes are located further away from the cylinder head, as shown in figure 4.2. When viewed from above, the holes are not aligned, such that a hole is positioned every 20°. The diesel hole diameter is 0.1 mm whereas, the hydrogen hole diameter is 0.6 mm. The umbrella for each of the fuels is the same and therefore, the diesel spray and gaseous hydrogen were injected parallel to each other. The HPDI injector is similar to the natural gas HPDI injector [65, 116]. The diesel pilot SOI occurs before the SOI of the main hydrogen injection, with a brief period of simultaneous injection. The pilot diesel contributes to approximately 5% of the total injected energy. The test case investigates three different SOI and two different rail pressures. The liquid/gas (diesel/hydrogen) rail pressures were 310/295 and 270/255 bar. The outline of the cases carried out is shown in Table 4.1.

Table 4.1: Computational and experimental cases and key injection parameters.

Case	Diesel/H2 SOI [°CA aTDC]	Diesel/H2 Duration CAD	Diesel/H_2 rail pressure [bar]
1	-9/-7	9/12.75	310/295
2	-9/-7	10.6/16.2	270/255
3	-5/-3	9.2/12.75	310/295
4	-5/-3	10.6/15	270/255
5	-1/1	9.6/15.4	310/295
6	-1/1	10.6/16.54	270/ 255

4.3.2 Simulation Set-up

The simulations for the hydrogen engine are carried out using CONVERGE CFD. The simulations carried out are closed cycle simulations from IVC to EVO, which are specified in these cases as -141 ° CA aTDC and 141° CA aTDC. A 40° sector of the full cylinder is used in the simulation to reduce the computational requirement. This sector domain captures one diesel nozzle and one hydrogen nozzle as seen in figure 4.3. The swirl acts in a counterclockwise direction in figure 4.3, and therefore, the green line indicates the interface output and the red line the interface.

The injection profiles for both the diesel spray and hydrogen gas jet are obtained from constant volume experimental measurements. Lagrangian particle tracking is used for the liquid spray with the KH-RT break-up model for the primary and secondary breakup. Since these models do not apply to gas injections, the hydrogen injection is modelled through a small pipe leading to the combustion chamber. At the inlet to this pipe, a mass flow rate is applied.

For the multiple injection of hydrogen cases, the general engine specifications are taken from the dual-fuel case described in Section 4.3.1. Case 1 from Table 4.1 was chosen as the base case for comparison with the pure hydrogen engine with a dual-fuel engine. The case remained the same except for the absence of the diesel injection. The main hydrogen injection was kept the same as the dual-fuel engine. The amount of pilot hydrogen injected into the chamber was increased to match the total amount of energy injected in the dual-fuel engine. The flow rate used in the dual-fuel case was used to form the pilot and main injection profiles, ensuring the opening and closing rates were similar. The amount of the pilot injection was adjusted to be 0.75, 2.5, 5, 10, 15 and 20% of the total injected energy. Three intake temperatures were investigated; 361, 376 and 391 K, corresponding to 0, +15 and +30 K from the dual-fuel cases, respectively. When adjusting the fuel temperature, the pressure was also adjusted to maintain the same global lambda.

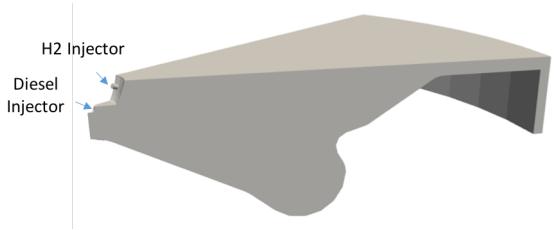

Figure 4.2: The sector of the hydrogen engine case with the location of the diesel and hydrogen holes.

The SAGE detailed chemistry model is used for the hydrogen-related engine simulations. For the dual-fuel simulations, the n-dodecane is injected as a surrogate for diesel. The n-dodecane reaction mechanism from Yao et al. [117] is used, containing 54 species and 269 reactions. For the hydrogen pilot simulations, a hydrogen reaction mechanism containing 21 species and 62 reactions is used [118].

Converge CFD solver uses an automatic meshing algorithm that can be controlled using fixed embedding regions and adaptive mesh refinement (AMR). Fixed embedding regions are used to refine the grid in specified areas within the domain and AMR automatically refines the grid based on the magnitude of the sub-grid field. The size of the refined cells in AMR is dictated by a base size. The same approach is used for all of the hydrogen engine cases. In the dual-fuel cases, two conical fixed embedding regions are located from the injector to the wall capturing both of the injection regions. Only one conical region is used for the hydrogen pilot case. Outside of this region, the mesh is refined using AMR based on temperature and velocity. The base size is 2mm, leading to a refinement size of 0.25mm in the fixed embedding regions and AMR.

4.4 Hydrogen Constant Volume Cases

4.4.1 Case Description

Diesel-hydrogen interaction was investigated in constant volume chamber experiments carried out by Rorimpandey et al. [85]. The chamber is a 114 mm cube with ambient temperature and pressure of 890 K and 52 bar, respectively. This work consists of an n-heptane pilot injection followed by a hydrogen main injection, with the pilot injection contributing to 6.4% of the total energy injected into the chamber. The fuels are injected through separate injectors with a reservoir pressure of 700 and 200 bar for n-heptane and hydrogen, respectively. The injectors are configured in a converging configuration as shown in Figure 4.4. As can be seen from the figure, the n-heptane injector is positioned 12.3 mm above the hydrogen and angled at 12°,

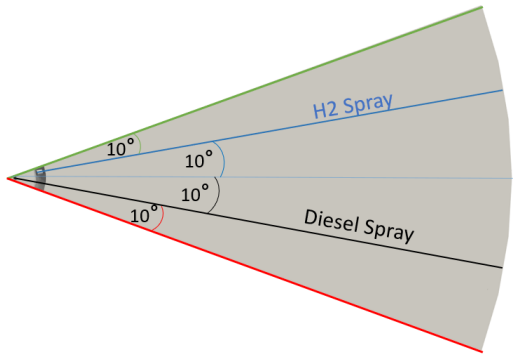

Figure 4.3: The top view of the hydrogen engine case show the direction of the fuel injection.

providing an intersecting axis of 57.2 mm into the chamber. The n-heptane injector hole diameter is 0.105 mm, and the hydrogen injector hole is 0.58 mm. The injection duration for the injections is 0.7 and 3.3 ms for n-heptane and hydrogen, respectively. For all of the experimental cases, the injection settings remain the same.

In the experimental work, the order of injection is changed, i.e., n-heptane-hydrogen or hydrogen-n-heptane, as well as the dwell time, which is measured as the time between hydraulic SOIs of each injection. The simulation focuses solely on the cases where n-heptane is injected first, which reduces the number of cases to three. The difference in these three cases is the dwell time, which is 0.93, 1.93, and 2.93 ms. The experimental data provided an aHRR inside the chamber and Schlieren imaging illustrating the spray/jet interaction and the combustion process.

4.4.2 Simulation Set-up

The numerical domain is a 114mm cube with a small pipe located in the centre of one of the surfaces acting as the hydrogen injector nozzle. This pipe has a diameter of 0.58 mm and a length of 1 mm, representing the physical distance nozzle distance [98]. At the entrance of this pipe, a mass flow boundary condition is applied. The applied injection profile is a trapezoidal shape with a ramp-up time of 0.3 ms and a ramp-down time of 0.05 ms. Between the ramp times, a constant flow rate of 1.56 mg/ms is used which is measured from experiments [98]. When changing the dwell time, only the SOI of the hydrogen injection is shifted. Since the diesel SOI occurs at 0 ms in the simulation, the dwell times are realised by using the hydrogen SOIs as 0.93, 1.93, and 2.93 ms. These timings account for any delay between the signal and the needle lift.

The n-heptane injection is modelled, and the virtual injector is positioned ac-

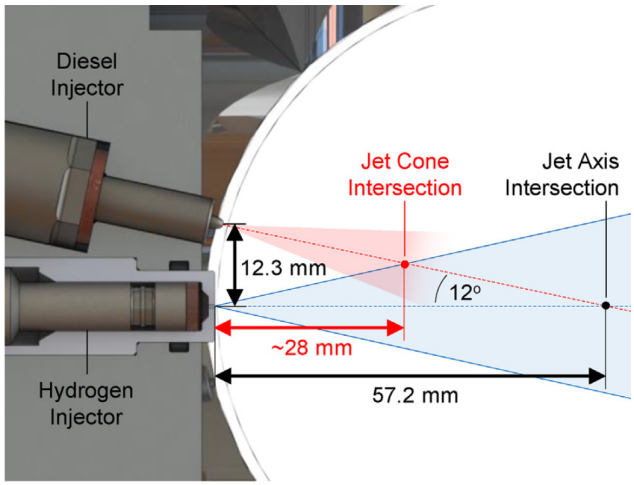

Figure 4.4: The injector configuration in the constant volume experiments. Reproduced from [85].

cording to Figure 4.4. The injector details are specified using the details given in the experimental work [85]. The injection profile for the diesel injection was obtained from the authors of the experimental work, which resulted in a total injected mass of 0.99 mg. The same injection profile profile was used for all cases. The SAGE detailed chemistry model is used along with an n-heptane mechanism including 54 species and 128 reactions [119].

These simulations are carried out using LES and therefore, special consideration for the mesh is required. The simulations are carried out in Converge CFD and therefore, a cartesian grid is used. In order to achieve a sufficiently fine grid in regions around each of the injections and the growing flame region, fixed embedding, and AMR are used as shown in Figure 4.5. A base grid of 4 mm is used covering regions outside of the fixed embedding and AMR regions. AMR is active on temperature, velocity and species of hydrogen and n-heptane. A conical fixed embedding region is located from the inlet of the hydrogen pipe to 15mm into the chamber, capturing the initial phase of the hydrogen jet. This embedded region contains a cell size of 0.0625 mm. This fixed embedding region is only active for the duration of the simulation and 0.05 ms after the end of injection (EOI). The diesel injection is treated differently, given the angle of the injector relative to the cell position and the much lower injection velocity compared to the hydrogen injection. Therefore, an inlaid mesh is used for the initial 15 mm of the n-heptane injection with a cell size of 0.125 mm. An inlaid mesh structures the cells so that they are positioned so that the cell faces are in the direction of the flow direction. Outside of the fixed embedding and inlaid mesh regions, AMR is in place on the temperature variable, adding cells of 0.125 mm, where a temperature change is observed.

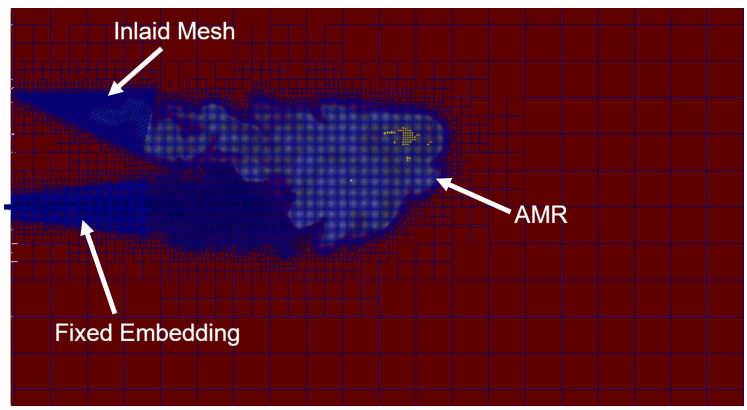

Figure 4.5: The inlaid, fixed embedding and AMR regions for the constant volume simulations.

Chapter 5

Results: Methanol

The main works in this thesis are separated by the fuel. This section will discuss the investigations of the methanol-fueled engine, which covers Papers I and II. Paper I carries out a comparison of methanol and iso-octane, a gasoline surrogate fuel, across HCCI and PPC ranges. Paper II focuses on methanol as the SOI is swept from HCCI to PPC ranges.

5.1 Comparison of methanol with iso-octane

5.1.1 Validation of CFD simualtions

A mesh study was carried out investigating three different grid sizes; coarse, medium and fine. During the mesh study, the same dynamic mesh algorithm was used for each mesh. The cell count at TDC for the coarse, medium and fine grids was 42,000, 65,000 and 121,000, respectively. Comparing the simulation pressure trace and aHRR with the experimental data showed that the coarse mesh predicted the onset of ignition too early. Additionally, the maximum pressure predicted by the simulation using the coarse was greater than the experiments. The medium and fine grids predicted very similar results which agreed with the experimental data. Since no improvement in the results was observed when using the fine grid, the medium grid was used for all simulations. The medium grid had an average cell size of 1.2 mm in the squish region and a refined size of 0.5 mm in the piston bowl region. This grid results in a very accurate prediction of pressure trace and aHRR in both the HCCI and PPC phase as shown in Figure 5.1.

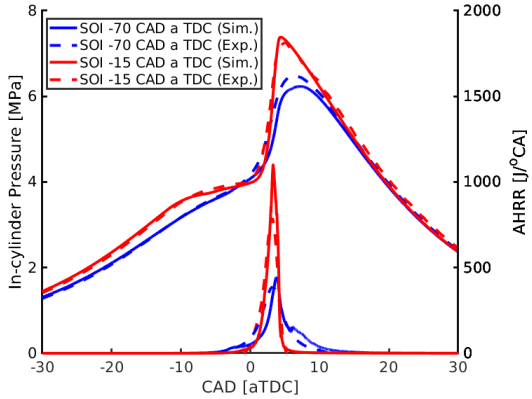

Figure 5.1: The pressure trace and aHRR for iso-octane (red) and methanol (blue) in the HCCI and PPC phase.

5.1.2 Intake Temperature

In Paper I, a direct comparison between methanol and iso-octane is carried out using the same engine conditions. As part of this study, the SOI is swept from -100° CA aTDC to -15° CA aTDC. This range covers HCCI to transition from HCCI to PPC and also the PPC operating regions. Throughout the simulations, the combustion phasing is kept constant at CA50 at approximately -15° CA aTDC. CA50 is the point at which 50% of the chemical energy has been released. This is done by adjusting the intake temperature. The resulting intake temperatures for each of the fuels can be seen in figure 5.2. Since the simulations carried out are closed-cycle, the precis intake temperature values are slightly different from the experimental measurements. The required intake temperature is notably higher than that of iso-octane. As mentioned in section 2.1.1, methanol experiences significant cooling during liquid evaporation. It can be determined that this higher intake temperature is a result of the cooling caused by this evaporation event that iso-octane does not experience.

Both of the fuels demonstrate the well-known 'spoon-shape' profile for intake temperature as the SOI is swept from HCCI to PPC modes. This spoon shape is caused by the different fuel-air mixtures that form as the SOI is adjusted. For early SOI, the handle of the spoon is formed. As the SOI is retarded, the intake temperature drops forming the spoons curve before again increasing to form the tip. When the fuel is injected early in the compression stroke, a significant amount of time is provided for the fuel to mix with the air before combustion occurs close to TDC. This significant amount of time produces a fuel-lean mixture which requires an increased intake temperature to ignite. As this mixing time is reduced, the mixture becomes less lean and, therefore, does not require such high intake temperatures for ignition.

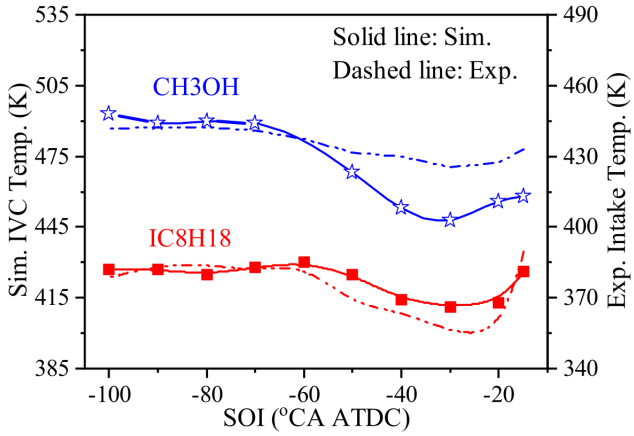

Figure 5.2: The intake temperatures for iso-octane (red) and methanol (blue) for both the simulation and the experiments.

For the late injection cases, a higher intake temperature is required to overcome the short mixing time. This short mixing time does not provide sufficient time for the fuel to heat up with a lower intake temperature.

5.1.3 Effect of SOI sweep

Early injection of the fuel can be problematic not just because of the increased risk of pre-ignition but also due to trapped fuel. Figure 5.3 shows the mass fraction of methanol 10 CAD after SOI of an HCCI and a PPC case. From the figure, the interaction of the HCCI case is seen to directly impinge around the region close to the crevice. As a result, fuel becomes trapped in the crevice and cannot be consumed in the main reaction that occurs in the piston bowl leading to increased emissions and decreased combustion efficiency. The late injection cases, also shown in this figure, do not suffer from the same issue since the injection is concentrated in the bowl region, making all of the injected fuel available for consumption in the combustion process.

Figure 5.4 show the equivalence ratio of methanol (left) and iso-octane right for HCCI, early PPC, and late PPC, respectively. Figure 5.4 illustrates the trapped fuel in the crevice close to TDC, whereas the remaining fuel that impinged on the cylinder liner is now located in the piston bowl. Comparing the two fuels, the mixture formation is quite different, where methanol has achieved a leaner mixture which has spread throughout the bowl, however, iso-octane has a more stratified mixture with a higher locally fuel-rich mixture. This trend is also observed in the PPC cases, where the iso-octane achieves a more stratified mixture with locally fuel-rich regions compared to methanol. These differences in mixture formation can be responsible for differences

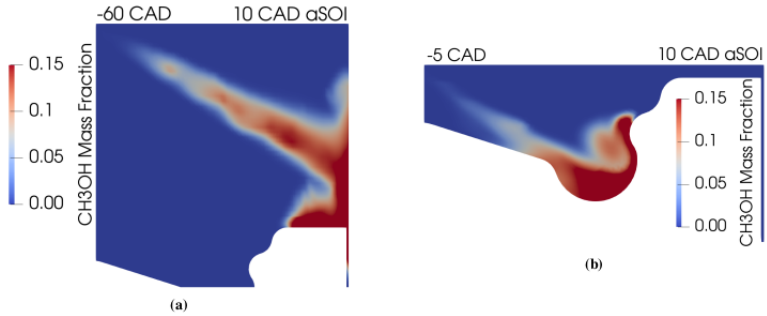

Figure 5.3: The mass fraction of methanol 10 CAD after SOI for (a) a HCCI case and (b) a PPC case.

in emissions and performance, which will be discussed in the following sections.

5.1.4 Performance

Figure 5.5 shows the trend for thermodynamic efficiencies and the losses that affect this efficiency for methanol across all of the SOIs. To begin, the combustion efficiency is highest in the late PPC range because all of the fuel is directed into the piston bowl and is consumed during combustion. As previously mentioned, the early injection causes fuel to become trapped in the crevice and, therefore, cannot be consumed, leading to higher combustion losses. The small rise in combustion losses as the SOI is retarded from -100° CA aTDC to -50° CA aTDC is due to the increased amount of trapped mass as the location of spray impingement approaches the crevice region. As soon as the location of the impingement is lower than the topland the combustion losses significantly drop.

It can also be observed that the heat losses are highest in the late PPC phase, where combustion efficiency is highest, leading to more heat released from combustion. Additionally, an important factor for heat loss is the location of the fuel and hence, the combustion. As observed in figure 5.4, the methanol is injected low in the piston bowl and is deflected along the piston surface. Investigating the combustion of the methanol shows that the ignition occurs at the tail end of the injection and follows the path of the methanol along the piston surface, greatly contributing to the heat losses. Overall, two key points can be identified as the highest thermodynamic efficiencies, -80° CA aTDC and -15° CA aTDC, with efficiencies of 39.87% and 41.96%, respectively. For the SOI=-80° CA aTDC case, the lower exhaust energy aids in overcoming the heat losses and high combustion losses. This exhaust energy is unused heat that is extracted from the cylinder into the exhaust. The thermodynamic efficiency in the SOI=-15° CA aTDC case benefits from the near-perfect combustion efficiency but suffers from the increasing heat losses as discussed. However, in this

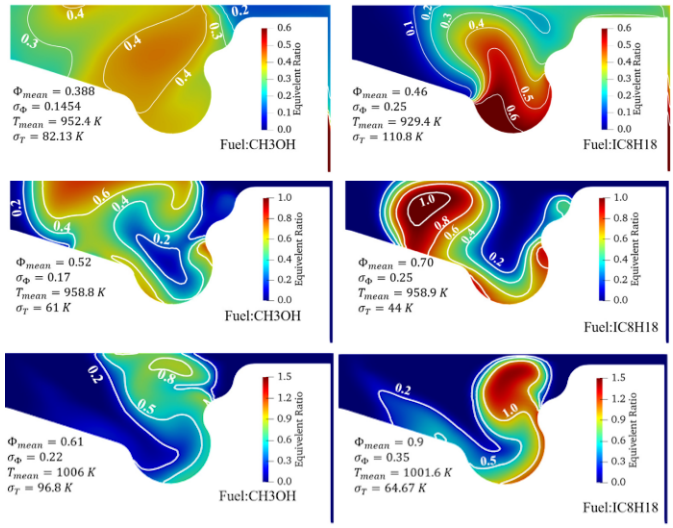

Figure 5.4: Top Row: The distribution of phi at -5° CA aTDC for iso-octane and methanol with an SOI of -80° CA aTDC. Middle Row: The distribution of phi at -5 ° CA aTDC for iso-octane and methanol with an SOI of -30° CA aTDC. Bottom Row: The distribution of phi at 0 ° CA aTDC for iso-octane and methanol with an SOI of -15° CA aTDC.

case, the exhaust loss sees a drop, caused by the low intake temperature, overcoming the other losses.

5.1.5 Emissions

The emissions for the methanol and iso-octane across the SOI sweep are shown in Figure 5.6. The experimental measurements for both fuels are shown in the left column, and the simulation is on the right. From the figure, it can be determined that the simulation predicts the experimental emissions trend very well. The emission of unburned hydrocarbons (UHC) follows the combustion efficiency trend very well, indicating that the trapped fuel is responsible. The NO_x emissions are at near-zero levels during the HCCI phase which is expected due to the fuel-lean mixtures providing a lower combustion temperature. Finally, the emission of CO is highest in the HCCI phase and sees a downward trend as the SOI is retarded. As mentioned, the early injection leads to fuel-lean mixtures which can lead to a longer combustion duration. During the combustion process, CO is oxidised into CO_2 with sufficient levels of O_2 and fast combustion duration. In the fuel-lean conditions of the SOI=-80° CA aTDC case, the combustion duration for methanol and iso-octane is 5.41 and 6.11 CAD, respectively. The later injection of the SOI=-15° CA aTDC cases, leads to a combustion duration of 2.32 and 2.41, respectively. In the early injection case, the excess air and long combustion duration is not sufficient for efficient oxidation of CO

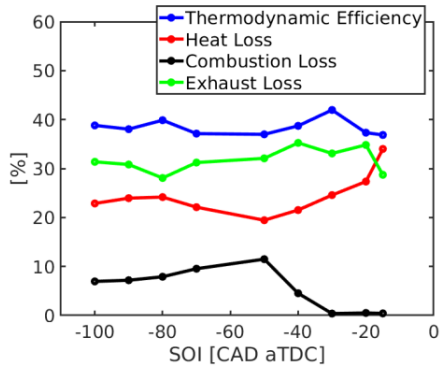

Figure 5.5: The thermodynamic efficiency, heat loss, combustion losses and exhaust losses across all investigated SOIs.

and therefore, CO emissions are high.

A more detailed presentation of the comparison between methanol and iso-octane is given in Paper I in the Appendix. A more focused presentation of the methanol results across the LTC ranges is given in Paper II in the Appendix.

5.2 Concluding Remarks

This work investigated the fuel/air mixing, ignition, combustion and pollutant emissions in methanol and iso-octane fueled DICI engines operating in different regimes of combustion: HCCI, PPC and CDC. It is found that a higher intake temperature was required for methanol, as compared with iso-octane, to counteract the high heat of vaporisation. As a result, the lower volumetric efficiency led to a consistently lower thermal efficiency when using methanol. Both fuels achieved the highest efficiencies across the sweep in the PCC phase at around -30 CAD aTDC. The fuel and air were more homogeneously mixed with methanol given the low stoichiometric AFR. High UHC emissions were observed in the HCCI region because fuel was trapped in the crevice region as a result of early injection. The larger fuel mass for methanol resulted in high UHC emissions in this phase. CO emissions in the methanol engine were lower than iso-octane engine due to the onset of ignition in fuel-lean conditions. The HCCI region for both fuels achieved near-zero NO_x emissions which increased as the SOI was retarded closer to TDC.

The simulations were able to predict the 'spoon shape' intake temperature profile as the SOI was shifted from HCCI to PCC. The changing intake temperature was required to achieve constant combustion phasing at different SOI for relevant mixture

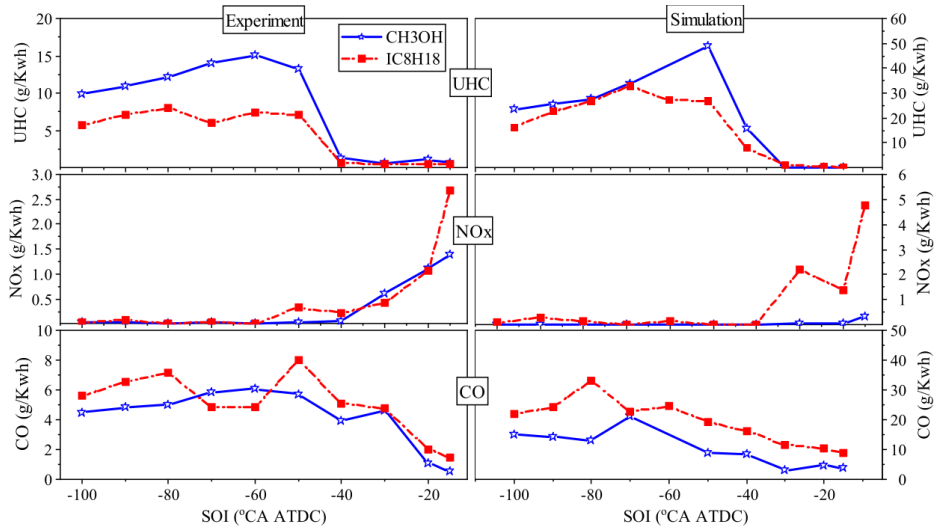

Figure 5.6: The emissions for methanol and iso-octane across the SOI sweep from the experiment (left) and simulation (right).

formations. The highest efficiency was observed in the PPC regime. In this regime, the combustion duration was the fastest due to the higher mixture stratification. Low combustion efficiency occurred in HCCI regime due to fuel being trapped in the crevice. High heat losses were observed for late SOIs due to the flame interaction with the piston surface. The more stratified mixture in PPC allowed for greater oxidation of CO. NO_x emissions remained low during the HCCI phase due to leaner mixtures and resulting lower temperature combustion. With SOIs close to TDC, NO_x emissions increased, due to the conventional diffusion flame combustion that yielded high flame temperature thus higher thermal NO formation.

Chapter 6

Results: Hydrogen

This section focuses on the investigation of hydrogen combustion both in a compression ignition ICE and in a constant volume chamber. First, the diesel hydrogen dual-fuel engine results will be presented. Second, based on one of the cases from the dual-fuel engine investigation, an investigation of multiple injection of hydrogen is carried out. Finally, a reacting constant volume study of diesel-hydrogen dual-fuel flames is investigated under compression ignition conditions. The investigations aim to address the research questions listed in Section 2.4.

6.1 Diesel-hydrogen Dual Fuel Engine

The Scania D13 heavy-duty CI engine with a compression ratio of 23 was studied at medium load conditions in experimental and numerical simulations to gain an improved understanding of the fuel/air mixing, in-cylinder flow, and combustion process. The experimental data at medium load are provided by Scania CV AB. The results are presented in Paper III in the appendix. In the following, highlights of the results are presented.

6.1.1 Validation of CFD simulations

A significant effort was applied during the validation phase of the CFD simulation of diesel-hydrogen dual-fuel engine cases to replicate the unique physics present in the engine. During the validation phase, many parameters were investigated including boundary conditions, models and mesh configurations. One of the biggest chal-

lenges faced in simulating hydrogen HPDI is the injection profile. As mentioned previously, hydrogen has the potential to have a varying flow rate depending on the NPR which can change rapidly, especially with large in-cylinder pressure change as a result of piston motion and combustion. This varying flow rate can be considered by: (i) including the injector geometry and applying the rail pressure at the inlet of the injector, (ii) determining the pressure losses through the injector and applying the injection pressure as the pressure boundary condition. Including the injector geometry is a complex task, requiring a very fine mesh for the small cavities in the injector. Additionally, this method would require the input of a needle motion profile, which would require special experimental measurements to determine, which furthermore, would likely vary with energising time, rail pressure and fuel mass as observed for natural gas injections [65, 116]. Using strategy (ii) would require accurate simulation to predict the pressure loss, which would rely on accurate simulation of the injector. Additionally, with varying a flow rate in the simulations, controlling the total injected energy is a challenge. For these reasons, it was decided to use a mass flow rate boundary condition. Many profiles were tested in reacting conditions and compared with the pressure trace and heat release rate from experiments. Ultimately, a mass flow rate obtained through constant volume experiments provided by Scania CV AB under similar conditions to the engine case was used, providing an accurate prediction of the pressure trace and heat release. Figure 6.1 shows the mass flow rate profiles for two cases listed in Table 4.1.

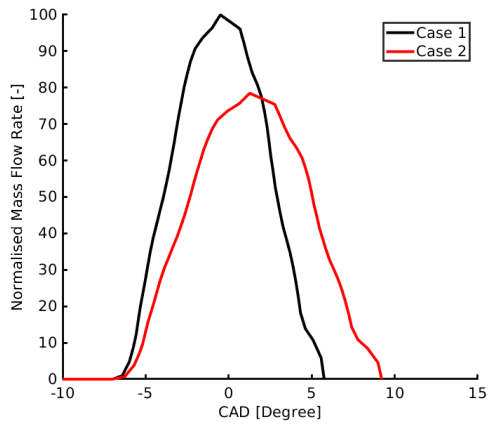

Figure 6.1: The mass flow rate profile determined from constant volume chamber experiments.

A mesh sensitivity study was carried out and compared with the experimental data. It was found that the AMR scale should be the same size as the fixed embedding scale to maintain a consistent cell size as the flame excited the fixed embedding region due to swirl. The mesh study carried out implemented the same base size of 2 mm for all cases; however, the refined region (AMR and fixed embedding) was varied to

0.5, 0.25 and 0.125 mm, representing a coarse, medium and fine grid, respectively. This results in a maximum number of cells for 170,000, 650,000 and 2,300,00 for the coarse, medium and fine grids, respectively. The resulting pressure trace is shown in Figure 6.2. The data is measured in all six cylinders and therefore, the cylinder with the minimum and maximum pressure is highlighted along with the average of the six cylinders. As can be seen in the figure, the medium and fine grids produce results within the min. and max. values. The computational time for the fine grid was approximately 150% of the required time for the medium grid to achieve a similar result. Comparing other parameters such as IMEP, CCE and ignition timing showed practically identical results. As a result, it was decided the medium mesh was sufficient for the remaining cases.

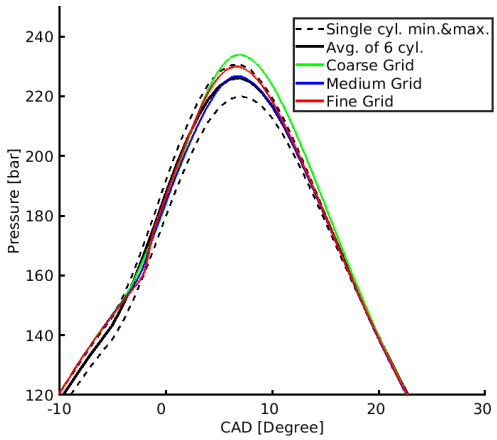

Figure 6.2: The experimental pressure trace for the cylinders with the minimum and maximum pressure trace as well as the average compared with the predicted trace from each of the grids.

6.1.2 Combustion Analysis

The following description of the combustion events is applicable to all cases investigated in this work. For all of the six cases (Table 4.1) presented, the time between the diesel injection and the hydrogen injection is constant. Figure 6.3 shows the combustion process following the injection of hydrogen. Since a single sector was simulated, the simulation data is reproduced and transformed to show a 80° sector to provide a clearer illustration. The dark grey regions here represent the periodic boundaries of the simulation. Figure 6.3(a) is 4.5 CAD after SOI of diesel and 2.5 CAD after SOI of hydrogen. Prior to this point, the diesel flame ignites almost immediately as it is injected into the combustion chamber, given the high compression ratio. In this figure, the diesel has fully ignited, and the hydrogen flame has become close enough to the hot diesel flame to show the onset of ignition on the underside of the jet.

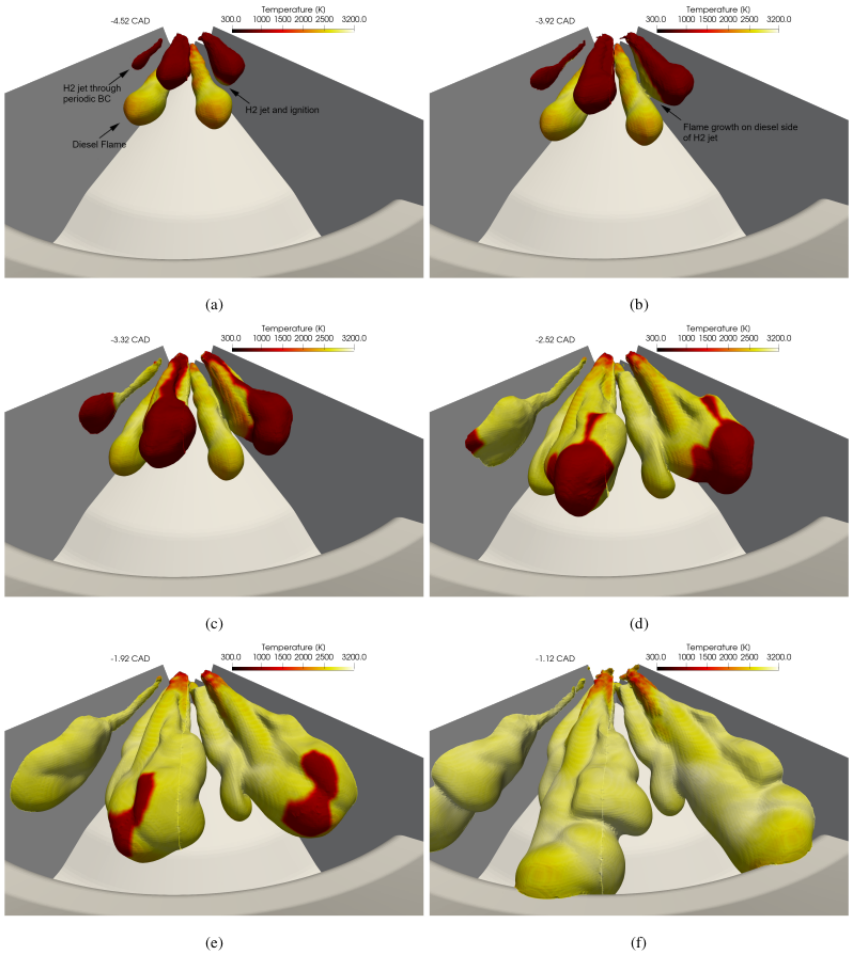

Figure 6.3: The iso-contours of phi=1 coloured by temperature across several CAD for the dual-fuel engine.

As both the diesel flame and hydrogen penetrate further into the combustion chamber, the hydrogen jet is exposed to a larger portion of the high-temperature diesel flame. In addition to this, both the spray and the jet grow radially. The high-temperature region on the hydrogen jet grows the fastest on the side closest to the diesel flame, as seen in Figure 6.3(b). At this point the flame spreads backwards towards the injector rather than around the circumference of the jet; however, it does not reduce the lift-off length to zero at this point. Once the flame has spread to cover the region closest to the diesel, it begins to spread around the circumference, as seen in Figure 6.3(c). One of the latest regions to ignite is the tip of the hydrogen jet which can be seen in Figures 6.3(d) and (e). However, just before interacting with the piston surface, the flame spreads, covering the entirety of the hydrogen jet. Since the injector configuration is such that the injector holes are parallel and offset when viewed from

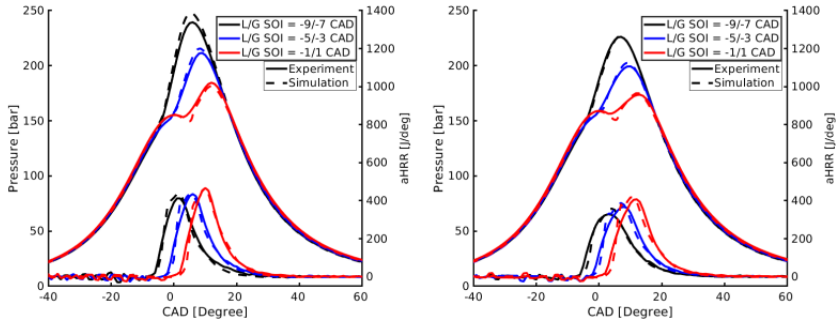

Figure 6.4: The experimental and simulation pressure trace and aHRR for the high rail pressure cases (left) and low rail pressure cases (right).

above, no high momentum interaction between the fuels is observed. However, as the hydrogen jet penetrates the cylinder the radial growth of the jet along with the swirl sees the diesel and hydrogen flame content as seen in Figures 6.3(d) through (f).

6.1.3 Engine performance

Figure 6.4 shows the pressure trace and aHRR for the experimental and simulations for each of the six cases listed in Table 4.1. The figure on the left represents the higher rail pressure, and on the right, the lower rail pressure. As can be seen, the simulation is able to predict the experiments with very good agreement. Each of the rail pressures is injected at three different timings. From the figure, it can be seen that early injection at the high rail pressure results in the highest in-cylinder pressure, with a decreasing trend as the SOIs are retarded. In general, the pressure is lower for the lower rail pressure cases, which can likely be associated with the longer combustion duration of the lower rail pressure.

The resulting efficiencies for all six cases can be seen in Figure 6.5. This figure includes the closed cycle efficiency (CCE) for the experiments and the simulations and also includes the brake thermal efficiency (BTE) only for the experiments. The BTE is expected to be lower than the CCE since the BTE accounts for additional losses that cannot be considered in closed-cycle simulations. Two simulation plots are presented for each of the NO_x models used in these cases. It can be seen from the figure that the simulation is able to predict the trend of decreasing efficiency across the cases which is confirmed by both the experimental CCE and BTE. It can be seen from the figure that the highest efficiency is achieved with the earliest SOIs. Additionally, it can be seen that the rail pressure does not have a significant impact on the efficiency, confirmed in Figure 6.6.

Figure 6.6 shows the energy balance for each of the cases, where combustion

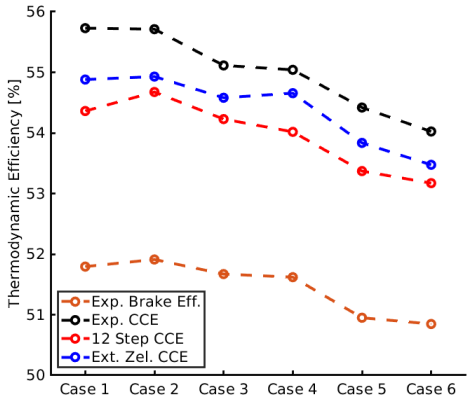

Figure 6.5: The CCE of the experiments and simulations and the BTE of the experiments.

losses are not included since it was measured to be zero. From this figure, it can be seen that the difference in work or thermodynamic efficiency can be associated with the change in exhaust loss as the SOI is retarded. The heat losses contribute only a small portion towards the losses; however, it is clear that the higher momentum of the high rail pressure provides a greater interaction with the piston surface leading to slightly more losses compared to the lower rail pressure. As the SOI is retarded, the heat losses decrease by approximately 2%. However, this is counteracted by the increasing exhaust losses, which see a rise of approximately 4%. The trade-off between the exhaust and heat losses can be associated with the 2% drop in work between Cases 1 and 6.

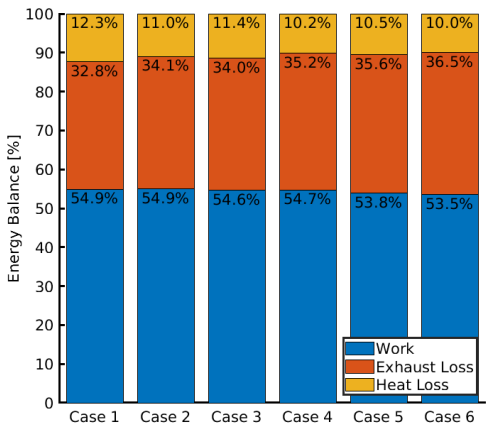

Figure 6.6: The energy balance for all six cases.

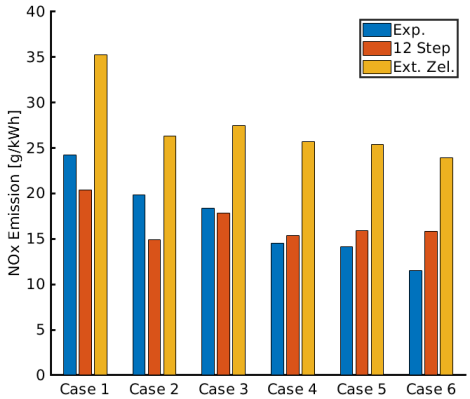

Figure 6.7: The NO_x emissions for all six cases from the experiment, Extended Zeldovich mechanism and 12-Step mechanism.

6.1.4 NO_x Emissions

NO_x are problematic in hydrogen engines given the high adiabatic flame temperature and fast laminar flame speed. As mentioned, in order to accurately capture the NO_x emissions correctly, two models were investigated. The resulting emission can be seen in Figure 6.7. It can be seen both models are able to capture the trend of NO_x emissions. However, the 12-step mechanism shows a better prediction of the amount. It can also be seen that the trend for NO_x emissions follows the same trend as efficiency, i.e., NO_x is highest where efficiency is highest.

The source of NO_x emissions is associated with high-temperature combustion regions. Figure 6.8 shows the equivalence ratio, temperature, and mass fraction of NO_x at CA50 for the high rail pressure cases. It can be seen that the in-cylinder temperatures reach significant temperatures. While the highest temperature regions are around ϕ=1 (stoichiometry), the highest concentration of NO_x is observed closer to the injector at this point, identified by point A in the figure. This point A can be associated with the diesel spray. This region can also be associated with the point where the hydrogen jet ignites from interacting with the diesel flame.

A more detailed presentation of the results is given in Paper III in the Appendix.

6.1.5 Concluding Remarks

This study investigates the diesel-hydrogen interaction in a dual-fuel DICI engine and identifies the impact of operating parameters on engine performance and emissions. It

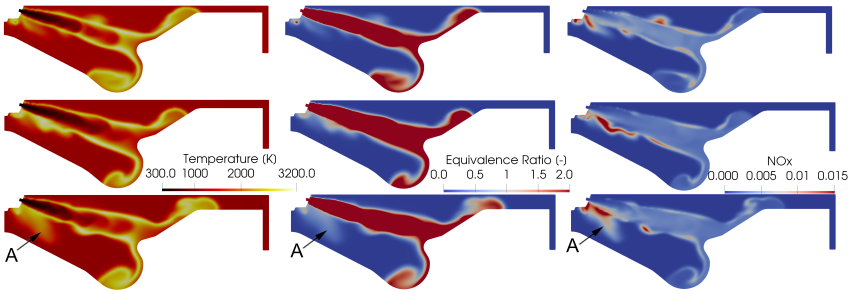

Figure 6.8: The equivalence ratio (left), temperature (center), and NO_x mass fraction right for Case 1, 3, and 5 (high rail pressure cases) at CA50.

is shown that the hydrogen ignites when it comes close to the high-temperature pilot flame, without any significant mixing of the fuels. The ignition of the hydrogen jet occurs on the side closest to the diesel flame and spreads quickly upstream and around the diameter of the jet. The highest efficiency was predicted for the earliest SOI and highest rail pressure, agreeing with the experiments. However, at this point, the flame temperature is highest producing the highest emission of NO_x. This trend of high efficiency, NO_x was observed throughout these cases. A significant contributor to decreased engine efficiency is the high exhaust gas temperatures, which increased with later injection. The Extended Zeldovich model for NO_x prediction results in a higher level of emissions than measured in the experiments. A 12-Step NO_x model provided a better prediction. Albeit this, both models were capable of predicting the overall trend of NO_x emission in the diesel-hydrogen dual fuel engine.

6.2 Single-Fuel Multiple Injection Hydrogen Engine

In this section, the multiple injection hydrogen engine strategies are investigated. As illustrated in methanol PPC engines, multiple injection of fuel has the potential to lower the ignition temperature due to the charge stratification. The baseline engine used in the study is the same Scania D13 engine with a compression ratio of 23. In particular, Case 1 from the dual-fuel cases listed in Table 4.1 is used as the baseline case for the hydrogen multiple injection investigation. The same boundary conditions and engine details are used except for the replacement of the diesel injection with the hydrogen pilot injection. Additionally, the intake temperature was adjusted as described below.

6.2.1 Intake temperature

To begin with, the SOI of the main injection (SOI_{main}) is fixed at -7° CA aTDC, and three intake temperatures (T_{IVC}) are used: 361K, 376K, and 391K. T_{IVC} of 361K comes from the dual-fuel cases above, and the other temperatures are +15K and +30K. When doing so, the pressure is adjusted so that the global lambda remains constant for all cases at 2.85. With these conditions, the various dwell times and pilot mass are investigated. Two parameters are evaluated: the ignition delay time (IDT) and the maximum pressure rise rate (MPRR). The former indicates the possibility of achieving reliable ignition, whereas the latter indicates the noise level. Too long of an IDT may cause failure of ignition or incomplete combustion, while a high MPRR means a high noise level.

The results of all of these cases can be summarised in Figure 6.9, which shows the IDT relative to the main injection and the MPRR. Many of the cases resulted in a very rapid rate of heat release, and therefore, a threshold for the MPRR of 10 Bar/CAD was put in place to outline which cases achieved controlled combustion in the cylinder. As can be seen from the figure, only a small number of cases achieved an MPRR within this limit, most of which at the increased intake temperature of 391K. It can be seen that without increasing T_{IVC}, none of the cases reach this limitation. This is due to the in-cylinder conditions not providing sufficient conditions for the ignition of the pilot, resulting in the premixed combustion of a large amount of fuel later in the cycle. The negative IDT in the figure occurs for pilot masses of 20%, releasing a large amount of heat immediately prior to the main injection SOI_{main}. The interaction between the high-temperature combustion and the main injection results in rapid ignition and subsequent heat release of the main injection.

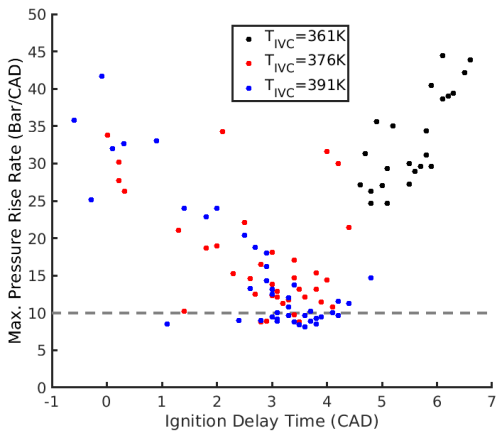

Figure 6.9: The ignition delay time against the maximum pressure rise rate for all cases investigated.

There is a special relationship between the pilot mass and the dwell time to achieve a constant MPRR or IDT. To find the optimal operation window, the dwell time must be tuned alongside the pilot mass. For example, providing a small pilot mass with a long dwell time will result in fuel-lean conditions that will not ignite. The same can be said for a large pilot fuel mass that is too short of an ignition delay time. This is shown in Figure 6.10, which outlines the MPRR for dwell times and pilot masses. The figure shows that the low pilot energy with the short dwell time or the high pilot energy with the long dwell time can achieve a reasonable MPRR. Increasing the IVC temperature can allow for a larger dwell time/pilot energy window to achieve a low MPRR.

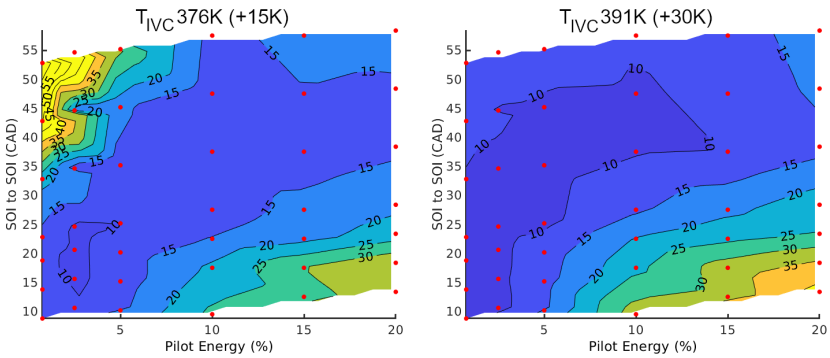

Figure 6.10: The MPRR for the dwell times and pilot energy shares for the intake temperatures of 376K and 391K.

However, increasing the IVC temperature has negative effects on the performance and emissions of the engine. Table 6.1 shows the engine performance and NO_x emissions for the increased intake temperature cases compared to the baseline dual-fuel case (H2DF). It can be seen that the engine efficiency of the hydrogen pilot cases is lower than the dual-fuel base case. This difference in efficiency can be due to the higher intake temperature that gives rise to high heat losses and exhaust losses since the combustion phasing is later and the higher temperature combustion observed in the cylinder. The higher combustion temperature and high flame speed of hydrogen resulted in higher NO_x. The highest intake temperature resulted in in-cylinder temperatures consistently higher by 40K.

Table 6.1: Engine performance parameters for the increased intake temperature using a pilot energy share of 2.5%.

Parameter (units)	H2DF	376K	391K
IMEP (Bar)	14.78	14.6	14.51
Efficiency (%)	54.45	52.96	52.6
NOx (g/kWh)	24.92	30.26	34.43
Peak Pressure (Bar)	228.7	232.7	238.4

6.2.2 Combustion Process

To understand the engine performance and emission, the combustion process is investigated for the case with a dwell time of 37 CAD with a pilot energy share of 2.5%. The selected case achieves an MPPR below 10 Bar/CAD, which is achieved at the intake temperature of 376K. Given the small pilot energy, the mass flow rate for the pilot is low yielding a short injection duration and, therefore, the penetration length of the pilot injection is very short. Given the low momentum of the hydrogen jet and the long IDT, the pilot is heavily affected by the swirl and forms a large region that reaches from the cylinder head towards the knee of the piston. Larger pilot energy shares experience a longer penetration length given the larger mass flow rate of these injections. With the early injection and longer penetration of the larger pilot mass, the fuel can become trapped in the crevice region.

At SOI_{main} (-7° CAD aTDC), the pilot injection has mixed with the surrounding air achieving an equivalence ratio of approximately 0.15 as shown in Figure 6.11. As the main injection enters the combustion chamber, low temperature combustion of the pilot occurs at -4.2° CAD aTDC in Figure 6.11. This is highlighted by the white line that surrounds the regions above 1200K. The location of this pilot combustion is directly positioned in the path of the main injection. Between -4.2° and -3° CAD aTDC, the size of the pilot combustion zone grows and is deformed by the main injection. At -3° CAD aTDC, the main injection arrives at the region where it interacts with the pilot. High temperature combustion of the main injection occurs due to the higher equivalence ratio. The high temperature flame spreads quickly to the tip of the jet of the main injection since the tip is surrounded by the deformed pilot flame. Simultaneously, the high temperature flame rapidly reduced the lift-off length on the upper side of the jet. Once the jet is surrounded in high temperature flame, it interacts with the stepped lip of the piston and separated into the bowl and towards the cylinder head.

6.2.3 Main injection timing

To improve the potential heating from the compression due to piston motion, the SOI_{main} was shifted to -1° CA aTDC. By doing so, a reasonable MPRR can be achieved without having to increase the T_{IVC}. However, a sufficient mixing time still must be provided for optimal ignition of the pilot. All the pilot injection cases investigated could ignite without an increased intake temperature; however, different dwell times were required. The engine performance for these cases is shown in Table 6.2. From the table, the peak pressure is measured to be lower than the dual fuel case shown in Table 6.1. A clear trend in increasing engine efficiency is observed as the

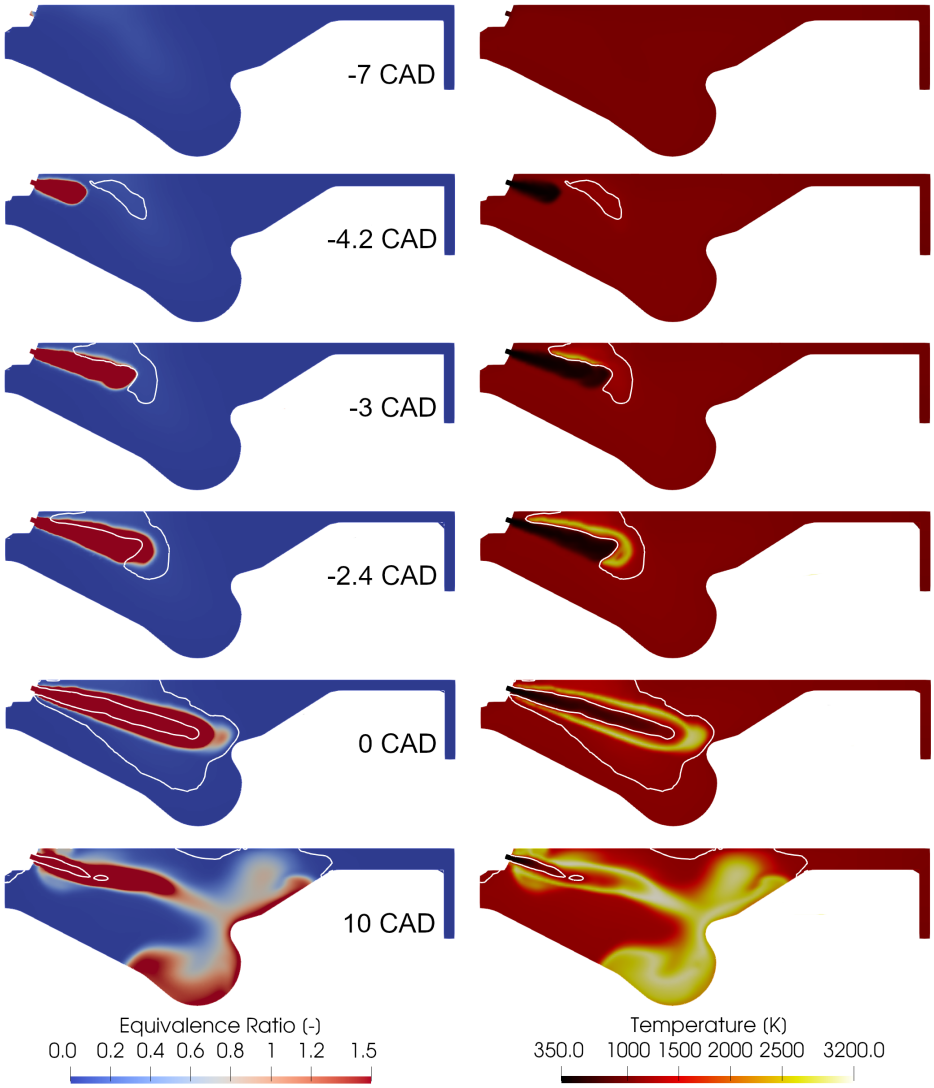

Figure 6.11: The equivalence ratio (left) and the temperature (right) illustrate the combustion process of the hydrogen pilot engine. The white line surrounds the region with temperatures above 1200K.

pilot energy share increases. However, these efficiencies do not reach the same 54% observed in the dual-fuel case or 52.96% from the increased intake temperature case in Table 6.1. It is likely these lower efficiencies are due to higher exhaust losses due to the later combustion phasing from the late injection, which was observed in the dual-fuel cases. However, the cases in Table 6.2 show a significant reduction in NO_x, which also decreases as efficiency increases. This reduction in NO_x can be associated to the larger amount of fuel burned in the low temperature premixed combustion

mode. The 20% pilot energy share resulted in an MPRR above 10 with the EOI-to-SOI time of 20 CAD. Increasing this gap to 30 CAD likely resulted in too fuel-lean pilot conditions. For this reason, the efficiency and NO_x trend is disrupted.

Table 6.2: Engine load, efficiency and NO_x emissions for the cases with SOI_{main}=-1 ° CA aTDC and $T_{IVC} = 361K$.

EOI to SOI (CAD)	15			20		30
Pilot Energy	0.75%	2.5%	5%	10%	15%	20%
IMEP (Bar)	14.32	14.35	14.41	14.45	14.52	14.2
Efficiency (%)	51.9	52.02	52.24	52.43	52.7	51.54
NOx (g/kWh)	21.25	20.9	20	18.7	17.4	18.3
Max. Pressure (Bar)	177	177	178.3	193	190	182

A more detailed presentation of the results is given in Paper IV in the Appendix.

6.2.4 Concluding remarks

This work demonstrated the potential for a carbon free heavy duty compression ignition engine based on pure hydrogen. With an early main injection of -7° CAD aTDC, an increase in the baseline intake temperature of at least 15K was required for controlled combustion. The IDT of the pilot must be controlled to provide sufficient combustion of the pilot flame before the ignition of the main injection. Increasing the intake temperature provides better conditions for the pilot to ignite, however, the overall engine efficiency is reduced due to the elevated wall heat loss and exhaust gas heat loss. Shifting the main injection to -1° CAD aTDC provides controlled combustion without the need for an increased intake temperature. Compared to the diesel-hydrogen dual-fuel baseline engine, the engine efficiency was slightly reduced however, the NO_x emission also decreased. The NO_x emission decreased as the pilot share increased due to the premixed combustion mode of the pilot. This finding is to be confirmed in future experiments; however, it sheds light on the development of future pure hydrogen engines.

6.3 Hydrogen Constant Volume Vessel

In this work, large eddy simulation was performed to study diesel-hydrogen interaction in a constant volume vessel under conditions relevant to diesel-hydrogen dual fuel DICI engines. The configuration was selected since experiments were available [85]. LES was chosen for the study to achieve better accuracy in capturing the mixing and combustion process than RANS. In both the experiments and LES, n-heptane was used to represent diesel.

6.3.1 Validation of CFD simulations

The details of the experimental conditions are well defined in the literature [98, 99]. As mentioned in Section 6.1.1, the HPDI process can be challenging due to the potentially varying flow rate as a result of NPR changes. However, in a constant volume chamber, the NPR does not change significantly and therefore, a mass flow rate boundary condition is optimal. For the given conditions, the steady-state flow rate was measured in the experiments to be 1.56 mg/ms [98]. Additionally, the ramp-up and ramp-down time were provided in the literature. The diesel injection profile was measured in the experiments and used directly in the simulations. The profiles for both fuels in Case I is shown in Figure 6.12. For the longer dwell times, the hydrogen injection is shifted along the x-axis.

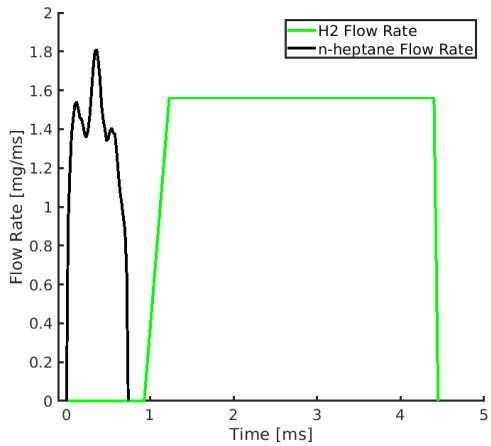

Figure 6.12: The flow rate for the n-heptane and hydrogen injections for the short dwell time.

Two different meshes were investigated as part of this study. The fine mesh used a cell size of 0.0625 mm in all of the refined regions (AMR and fixed embedding). The second mesh is described in Section 4.4.2. Both of the meshes predicted a similar heat release during the n-heptane combustion. Similarly, the prediction of the ignition was similar for both meshes. The computational requirement for the fine mesh was significantly higher than the medium mesh. The medium mesh had a maximum cell count of 30 million cells at the end of the simulation. However, following the ignition of the hydrogen jet, the fine grid had a cell count of approximately 50 million. Further penetration of the hydrogen jet would see this rise significantly. Since the meshes produced a similar result, the medium grid was used.

6.3.2 Comparison with Experiments

The experimental work carries out Schlieren imaging on the chamber, capturing the injection of both fuels and the high-temperature flame. Figure 6.13 shows the experimental Schlieren imaging compared to images from the simulation at the same time for the dwell time of 0.93 ms. The red and blue outlines on the experimental imaging highlight the n-heptane and hydrogen injection volumes, respectively. The green outline represents a high-temperature volume. The n-heptane ignition and initial phase of combustion are well captured by the simulation. However, it does not predict the same lift-off length observed in the experiment. In fact, the simulations do not predict a near-zero lift-off length, as shown in the experimental Schlieren imaging. The reason for this could be the under-prediction of the radial expansions and the shear layer mixing around the jet core, which can prevent the flame from spreading into the fuel-rich region. The velocity in the jet core is approximately 2000 m/s, which can contribute to a high scalar dissipation in this region. As a result, local flame extinction could occur, preventing the flame from propagating to the nozzle [120]. Furthermore, the local flow speed could be greater than the propagation speed, forming a border where the flame cannot pass [121, 122], or the local flow residence time is too short for the ignition of the hydrogen jet close to the nozzle [123].

Immediately following the jet core, the axial velocity drops rapidly, and the radial growth increases. In this region, strong levels of mixing begin in this region and increase as the distance from the nozzle increases. As the jet penetrates further into the chamber, the jet core remains the same length but the very low mixing region at the jet tip grows larger. This jet tip region is one of the first regions to interact with n-heptane flame and therefore, where ignition occurs.

The simulation and experimental aHRR for three dwell times are shown in Figure 6.14. All of the experimental runs are included in the figures: five for the short and medium dwell time and four for the long dwell time. The experimental and simulation aHRR is calculated from the pressure trace following the same procedure. Run-to-run variations are observed in the experiments. These variations are prominent in the n-heptane combustion phase and the pre-mixed combustion phase of the hydrogen, especially for the 2.93ms dwell time. It is observed that the IDT for the n-heptane combustion is different between each of the dwell times. This is confirmed by the reported IDTs from the experiments of 0.58 ± 0.09, 0.69 ± 0.03, and 0.66 ± 0.09 ms for the dwell times of 0.93, 1.93, and 2.93 ms, respectively. This variation in aHRR and IDT can be a result of fluctuations of flow and thermodynamic variables in the combustion chamber, such as hot spots, which are not present in the simulation, given the homogeneous initial conditions. Similarly, differences in the steady-state combustion phase can be caused by slightly larger hydrogen mass flow rates.

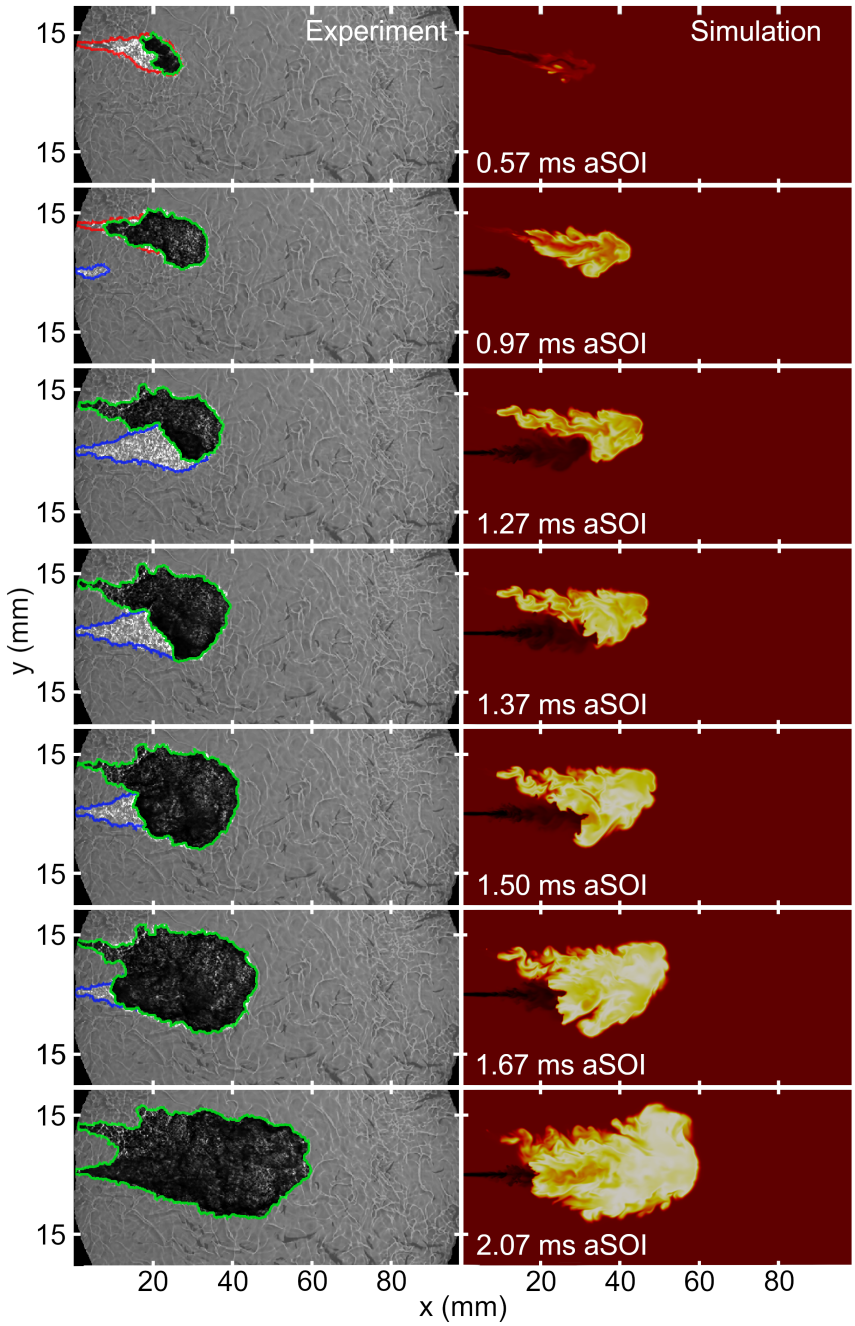

Figure 6.13: The comparison of the experimental Schlieren images with the corresponding simulation images for the short dwell time.

In these heat release figures, the pilot and main combustion phases can be identified. The pilot combustion is identified by the small bump at the beginning of the plot injection since only a small amount of energy is injected here. For all cases, the pilot combustion has begun before hydrogen injection begins, as already shown in Figure 6.13. The combustion of the hydrogen fuel can be separated into a premixed phase, identified by the large peak, and a non-premixed phase, which is the relatively consistent heat release phase following the peak. The premixed peak grows larger as the dwell time increases because a larger time is provided for the premixed region to grow before it is ignited.

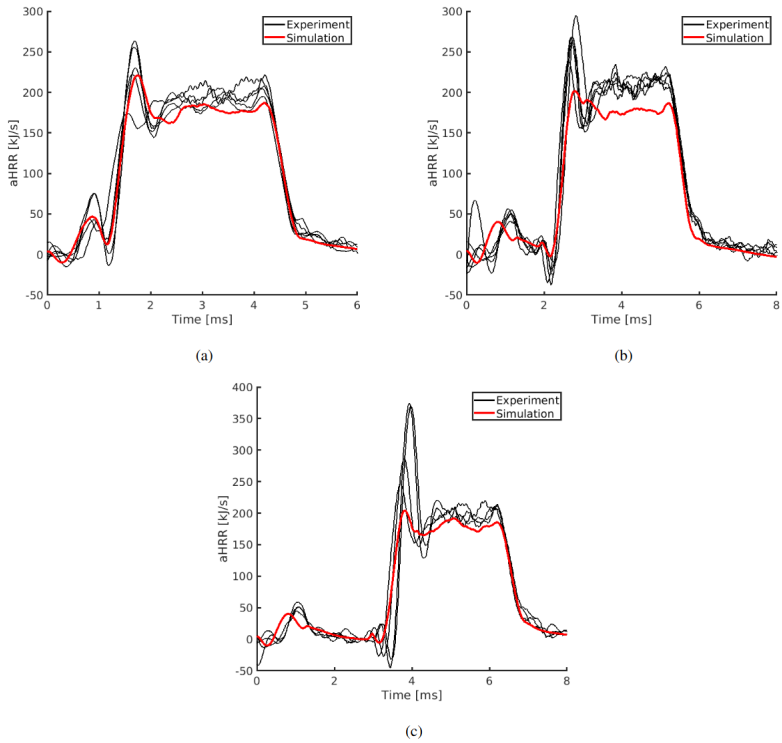

Figure 6.14: (a) The aHRR for the dwell time of 0.93 ms. (b) The aHRR for the dwell time of 1.93 ms. (c) The aHRR for the dwell time of 2.93 ms.

6.3.3 H2 Ignition

The Phi-T diagram in Figure 6.15 shows the ignition process of the hydrogen jet for the short dwell time case. The figures are colored by C/H ratio such that the fuels can be identified. Values above 5 represent the ambient composition formed in the pre-burn procedure. Values close to zero represent the hydrogen jet (due to zero carbon in the mixture), and the diesel mixture is represented by approximately 2 to 4. Figure 6.18

can be used as a reference. The Phi-T diagram shows that the mixing of the hydrogen and diesel occurs at approximately $\phi = 0.6$. This interaction first occurs in the cooler sections of the diesel flame. As the mixing continues, the temperature of this mixture increases at the same value of ϕ which is identified at times 1.34 and 1.35 ms. Once the diesel/hydrogen mixture undergoes high temperature combustion, the flame quickly spreads to the pure hydrogen region indicated by dark blue. It can also be noted from this figure that the peak temperature occurs at phi values slightly above 1.

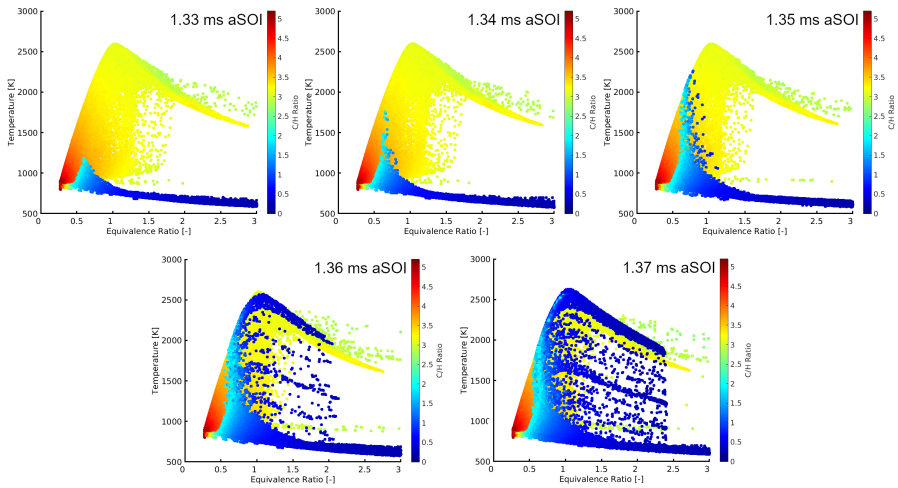

Figure 6.15: Phi-T diagram throughout the ignition process of the short dwell case. The points are colored by C/H ratio where 0 indicates pure hydrogen.

The ignition procedure described above is the same for all cases; however, the length of the process increases as the dwell time increases. Notably, the initial heating of the diesel/hydrogen mixture occurs consistently at the same phi value. By increasing the dwell time, more time is dedicated to the uninterrupted combustion of the n-heptane pilot fuel and cooling the flame in the surrounding air. Figure 6.16 shows the pilot flame for each dwell time immediately before the hydrogen ignition. As can be seen from the figure, increasing the dwell time leads to a difference in the temperature of the flame, with which the hydrogen interacts. The ignition of the hydrogen is impacted not only because of the local temperature of the flame but also because of the location of the flame in which the jet interacts. It is observed that for the long dwell time, the pilot flame has a relatively high temperature at the tip, but the hydrogen flame interacts further back in a locally cooler region.

As observed in the Phi-T diagram, some level of mixing between the hydrogen jet and pilot flame occurs. As the dwell time is increased, the mixing time is longer because of the local flame temperature. Additionally, the hydrogen flame is observed to perturb the pilot flame, observed clearly on the short dwell time of Figure 6.16. The

time between the interaction of the jet and flame was measured to be 0.05, 0.08, and 0.15 ms for the short, medium, and long dwell times, respectively. This long mixing time for the long dwell time case is the reason for the large heat release peak in the premixed combustion phase.

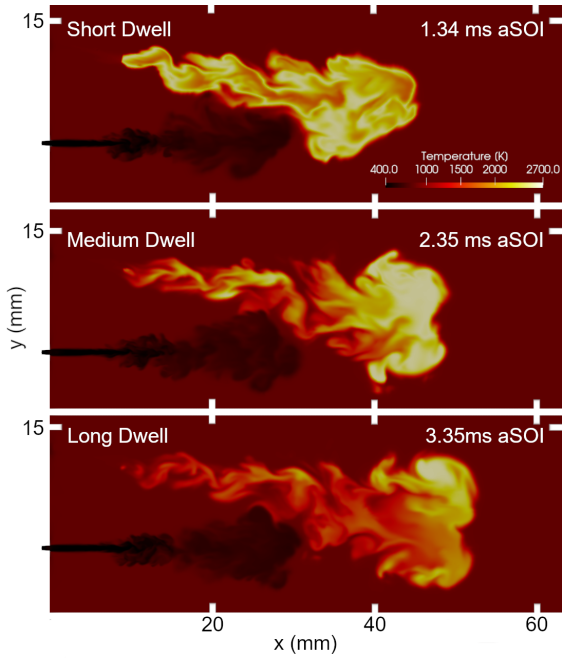

Figure 6.16: The state of the n-heptane flame prior to hydrogen ignition for each of the dwell times.

6.3.4 NO_x Emissions

As mentioned previously, NO_x emissions are a significant challenge in hydrogen combustion, and understanding their formation in dual-fuel applications can aid in reducing NO_x. The rate of NO_x production for each of the dwell time cases is shown in Figure 6.17. This figure shows that the rate of production is not directly impacted by the dwell time since the medium dwell time case produces the highest NO_x emissions. The total NO_x emissions produced during the combustion phase are 0.7134, 0.7889, and 0.6942 mg for the dwell times of 0.93, 1.93, and 2.93 ms, respectively.

The time at which this high NO_x region occurs towards the end of the hydrogen injection duration. The NO_x production is concentrated in the tip of the hydrogen jet, as shown in Figure 6.18. At this time, the pilot combustion is complete, and diffusion combustion of the hydrogen is the dominant combustion mode. However, it can be observed that the highest source of NO_x is on the side of the hydrogen

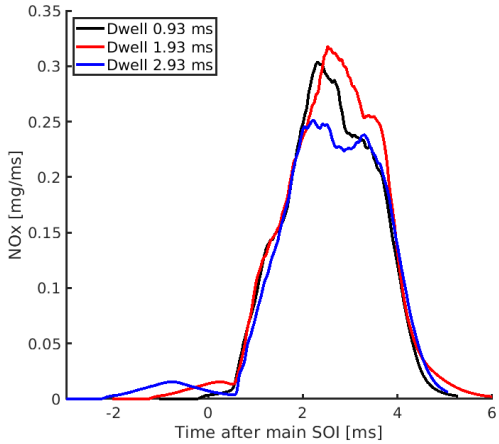

Figure 6.17: The rate of NO_x emissions for each of the dwell relative to the hydrogen injection SOI.

jet, where it interacts with the n-heptane pilot. From this observation, it can be determined that the direct interaction of the fuels impacts the NO_x, minimising the production of NO_x where the fuels have mixed. The figure shows the data from the short dwell case, and therefore, it can be determined that the long time between interaction and ignition of the hydrogen flame in the long dwell time case significantly contributes to the low formation of NO_x. The formation of NO_x was observed to be in the remnants of the diesel flame i.e. section of the flame with high carbon content.

A more detailed presentation of the results from LES is given in Paper V in the Appendix.

6.3.5 Concluding Remarks

LES is performed to investigate the interaction of n-heptane and hydrogen under conditions relevant to diesel-hydrogen dual-fuel DICI engines. The investigation encompasses cases with different dwell times, aiming to bridge the knowledge gaps identified in Section 2.4 regarding the dual fuel interaction.

It is found that the ignition of the hydrogen jet occurs once the tip of the jet reaches the diesel flame. The dwell time shows a significant impact on the combustion and emission process. With short dwell time, the ignition of the hydrogen jet is rapid and nearly immediately upon mixing with the diesel flame. With a long dwell time, the ignition is slower due to the diesel flame being cooled down by the ambient air before the interaction with the hydrogen jet.

The dwell time has a significant impact on the heat release rate and NOx for-

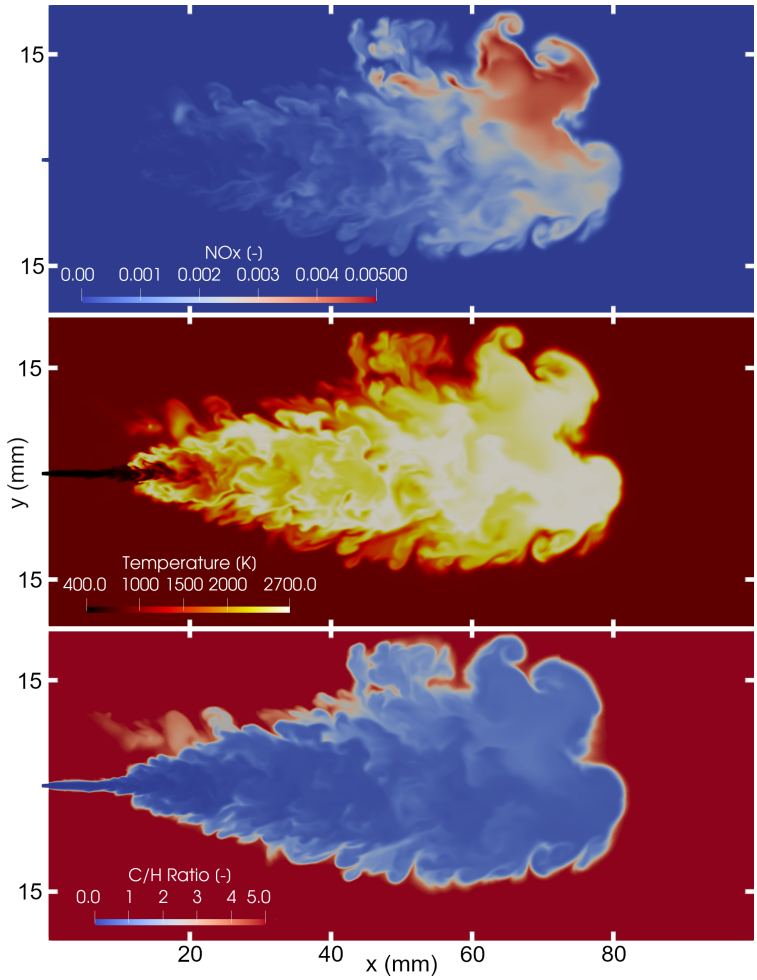

Figure 6.18: The mass fraction of NO_x, temperature and C/H ratio for the short dwell time at the point of peak NO_x production.

mation rate. The long dwell time allows more hydrogen/air to mix with the hot gas of the diesel flame, resulting in a high heat release rate. On the other hand, a high NOx region is found in the mixing region of the hydrogen jet and the diesel flame. A cooler diesel flame in the long dwell time case results in a lower flame temperature in large regions, which results in a lower NOx formation rate. The medium dwell time case shows the highest NOx formation rate due to the larger portion of the fuel/air mixture being around stoichiometry and, thus, high flame temperature.

The onset of diesel ignition is at the spray tip due to the long residence time and low scalar dissipation rate in the region. The onset of hydrogen ignition is also at the jet tip due to the direct mixing with the diesel flames. The flames in both the diesel jet

and hydrogen jet propagate upstream toward the nozzle. LES predicted a short lift-off length for both flames, which is longer than that observed in the Schlieren images. This difference is likely due to the over-prediction of the local scalar dissipation rate and the under-prediction of the jet spreading in the radial direction.

Chapter 7

Summary

7.1 Concluding Remarks

The first section of this thesis investigated methanol as a potential fuel for LTC strategies, sweeping the SOI from the HCCI range to the late PPC range. Methanol is a suitable candidate for LTC strategies given some of its chemical properties such as the high heat of vaporisation. The simulations were able to accurately predict the trends observed in the experimental work, including the 'spoon shape' profile for intake temperature. The changing intake temperature was necessary for maintaining the combustion phasing of CA50 at 3° CA aTDC. The difference in SOI leads to significantly different fuel-air mixture formations requiring unique intake temperatures to match the combustion phasing. For early injection cases, fuel became trapped in the crevice region and could not be consumed in the combustion process, leading to poor combustion efficiency and high emission of unburned hydrocarbons. When comparing methanol under LTC conditions with gasoline, methanol achieved fuel-leaner mixtures compared to iso-octane that was more stratified. For both fuels, NO_x emissions were at near-zero levels for the early injection cases of both fuels as a result of the lower in-cylinder temperatures from the local fuel-leaner mixture obtained through the longer mixing time. As this mixing time was decreased in the PPC phase, the NO_x emissions increased due to the high flame temperature at the close-to-stoichiometric mixture. CO emissions were overall lower for methanol compared to iso-octane and observed a downward trend as the SOI was retarded, due to improved oxidation.

The second part of the thesis focused on hydrogen combustion in compression ignition engines using dual-fuel strategies and single-fuel multiple injection strategies. This was achieved by completing engine simulations and LES of dual-fuel strategies in

a constant volume. In the dual-fuel cases, two rail pressures were investigated at three different SOI timings. The simulations were able to accurately predict the experimental pressure trace and apparent heat release. Given the parallel injector configuration in the dual-fuel cases, the diesel spray and hydrogen do not directly interact with each other; instead, the hydrogen comes sufficiently close to the diesel flame to ignite. From the cases investigated the early injection with high rail pressure provided the highest thermodynamic efficiency. From the cases investigated, a decreasing trend in efficiency was observed as the SOI was retarded, which was due to the increased exhaust losses. The NO_x emissions were investigated using two different models, both of which were capable of capturing the trend, but the 12-step model better predicted the magnitude of emissions. In this investigation, a relationship between NO_x and efficiency was observed where high efficiency was associated with high NO_x.

A dual-fuel case provided the foundation for a continuation study where the diesel is removed from the system, and combustion is obtained by splitting the hydrogen injection into a small pilot injection and a main injection. With a main injection timing of -7 ° CA aTDC, the intake temperature was shown to increase by at least 15K to provide sufficient conditions to ignite the hydrogen pilot. With this intake temperature only the smallest pilot energy cases was shown to result in stable ignition and also acceptable peak pressure rise rate; however, by increasing the intake temperature to +30K, the operating window was expanded at the expense of engine efficiency. By altering the dwell time and pilot energy share, a unique relationship was discovered, which requires optimisation to ensure an ignitable mixture can be achieved before the main injection. To be able to achieve controlled combustion using a hydrogen pilot without having to increase the intake temperature, the main injection timing should be delayed close to TDC. It is shown that shifting the main injection SOI from -7° CA aTDC to -1° CA aTDC enabled controlled combustion without having to increase the intake temperature. In these cases, a larger pilot energy share resulted in higher efficiency and lower NO_x emission. By using a larger pilot energy share, a larger portion of the injection fuel can be burned under pre-mixed combustion, where NO_x formation is low. However, this was only observed for pilot energy shares up to 5% because the dwell time proved to be insufficient for larger pilot energy shares.

The interaction of fuels in a diesel-hydrogen dual fuel DICI engine was investigated using large eddy simulation. It is found that hydrogen ignition upon its direct mixing with the diesel flame, due to the low ignition energy of hydrogen. The dwell time between diesel injection and hydrogen injection plays an important role in the combustion and emission process. The dwell time enables different times for the hydrogen/air mixing, and also for the entrainment of air to the diesel flame. A long dwell time tends to have low NOx emission due to the entrainment of cold air to the diesel flame allowing for a low flame temperature.

7.2 Future Work

Hydrogen compression ignition engines have not been well investigated until recently and therefore, there is significant potential for future work.

- A larger number of parameters can be investigated to fully optimise the dual-fuel engines, such as injector configuration and piston bowl design. Liquid and gaseous sprays have been demonstrated to behave differently; therefore, designing a piston bowl, particularly for hydrogen combustion, could positively impact combustion.
- For the diesel-hydrogen dual-fuel engines, a critical point would be to minimise the amount of diesel injected into the system. One method to do this could be to reduce the number of diesel holes in the injector, however, this would likely have an impact on the combustion of the hydrogen jet which needs to be investigated.
- The best scenario for hydrogen ICEs is to maintain the compression ignition engine but eliminate the need for an additional fuel, hence, eliminating carbon from the system. The CFD simulations in this work identified an operating window for the pure hydrogen (hydrogen pilot) cases. To confirm this operating window and the potential for this strategy, engine experiments should be carried out. Such an investigation can be efficiently carried out using CFD simulations to identify a particular design that can be experimentally tested.
- A challenge associated with hydrogen combustion is the high levels of NO_x emissions. For hydrogen engines to successfully replace diesel engines, a significant focus should be placed on reducing NO_x emissions at the source.

References

[1] N. Oceanic, A. A. (NOAA), Monthly Global Climate Report for Annual 2023, 2024.
URL https://www.ncei.noaa.gov/access/monitoring/monthly-report/global/202313

[2] H. Ritchie, P. Rosado, M. Roser, Emissions by sector: where do greenhouse gases come from?, Our World in DataHttps://ourworldindata.org/emissions-by-sector (2020).

[3] E. Commission, Commission regulation (eu) 2016/646 of 20 april 2016 amending regulation (ec) no 692/2008 as regards emissions from light passenger and commercial vehicles (euro 6) COM (2016) 1792 (2016).

[4] European Commission, Regulation of the european parliament and of the council on type-approval of motor vehicles and engines and of systems, components and separate technical units intended for such vehicles, with respect to their emissions and battery durability (euro 7) and repealing regulations (ec) no 715/2007 and (ec) no 595/2009 COM (2022) 595 (2022).

[5] I. E. A. (IEA), World Energy Outlook 2023, 2023.

[6] H. Liimatainen, O. van Vliet, D. Aplyn, The potential of electric trucks – an international commodity-level analysis, Applied Energy 236 (2019) 804–814.

[7] İ. A. Reşitoğlu, K. Altinişik, A. Keskin, The pollutant emissions from diesel-engine vehicles and exhaust aftertreatment systems, Clean Technologies and Environmental Policy 17 (1) (2015) 15–27.

[8] Y. Bi, J. Yan, S. Liu, B. Xiao, L. Shen, P. Wang, X. Nie, Study on diesel engine selective catalytic reduction performance at different atmospheric pressures using the response surface method, ACS Omega 8 (16) (2023) 14549–14557.

[9] A. K. Agarwal, A. P. Singh, R. K. Maurya, Evolution, challenges and path forward for low temperature combustion engines, Progress in Energy and Combustion Science 61 (2017) 1–56.

[10] J. Thangaraja, C. Kannan, Effect of exhaust gas recirculation on advanced diesel combustion and alternate fuels - a review, Applied Energy 180 (2016) 169–184.

[11] S. Frankl, S. Gleis, S. Karmann, M. Prager, G. Wachtmeister, Investigation of ammonia and hydrogen as co2-free fuels for heavy duty engines using a high pressure dual fuel combustion process, International Journal of Engine Research 22 (10) (2021) 3196–3208.

[12] P. Dimitriou, T. Tsujimura, A review of hydrogen as a compression ignition engine fuel, International Journal of Hydrogen Energy 42 (38) (2017) 24470–24486.

[13] J. Turner, G. Sverdrup, M. K. Mann, P.-C. Maness, B. Kroposki, M. Ghirardi, R. J. Evans, D. Blake, Renewable hydrogen production, International Journal of Energy Research 32 (5) (2008) 379–407.

[14] M. K. Singla, P. Nijhawan, A. S. Oberoi, Hydrogen fuel and fuel cell technology for cleaner future: a review, Environmental Science and Pollution Research 28 (13) (2021) 15607–15626.

[15] Y. Manoharan, S. E. Hosseini, B. Butler, H. Alzhahrani, B. T. F. Senior, T. Ashuri, J. Krohn, Hydrogen fuel cell vehicles; current status and future prospect, Applied Sciences 9 (11) (2019).

[16] J. Eggers, E. Villermaux, Physics of liquid jets, Reports on Progress in Physics 71 (3) (2008) 036601.

[17] J. E. Dec, C. Espey, Chemiluminescence imaging of autoignition in a di diesel engine, in: International Fall Fuels and Lubricants Meeting and Exposition, SAE International, 1998.

[18] J. E. Dec, A conceptual model of di diesel combustion based on laser-sheet imaging*, in: International Congress Exposition, SAE International, 1997.

[19] E. Svensson, C. Li, S. Shamun, B. Johansson, M. Tuner, C. Perlman, H. Lehtiniemi, F. Mauss, Potential levels of soot, nox, hc and co for methanol combustion, in: SAE 2016 World Congress and Exhibition, SAE International, 2016.

[20] D. Ravikumar, G. Keoleian, S. Miller, The environmental opportunity cost of using renewable energy for carbon capture and utilization for methanol production, Applied Energy 279 (2020) 115770.

[21] B. Johansson, S. Shamun, M. Shen, M. Tuner, J. Pagels, A. Gudmundsson, P. Tunestal, Exhaust pm emissions analysis of alcohol fueled heavy-duty engine utilizing ppc, SAE International Journal of Engines 9 (4) (2016) 2142–2152.

[22] Z. Tian, Y. Wang, X. Zhen, Z. Liu, The effect of methanol production and application in internal combustion engines on emissions in the context of carbon neutrality: A review, Fuel 320 (2022) 123902.

[23] S. Verhelst, J. W. Turner, L. Sileghem, J. Vancoillie, Methanol as a fuel for internal combustion engines, Prog. Energy Combust. Sci. 70 (2019) 43–88.

[24] S. Verhelst, T. Wallner, Hydrogen-fueled internal combustion engines, Progress in Energy and Combustion Science 35 (6) (2009) 490–527.

[25] P. J. Megía, A. J. Vizcaíno, J. A. Calles, A. Carrero, Hydrogen production technologies: From fossil fuels toward renewable sources. a mini review, Energy & Fuels 35 (20) (2021) 16403–16415.

[26] P. Nikolaidis, A. Poullikkas, A comparative overview of hydrogen production processes, Renewable and Sustainable Energy Reviews 67 (2017) 597–611.

[27] F. Dawood, M. Anda, G. Shafiullah, Hydrogen production for energy: An overview, International Journal of Hydrogen Energy 45 (7) (2020) 3847–3869.

[28] C.-C. Cormos, Hydrogen production from fossil fuels with carbon capture and storage based on chemical looping systems, International Journal of Hydrogen Energy 36 (10) (2011) 5960–5971.

[29] K. T. Møller, T. R. Jensen, E. Akiba, H. wen Li, Hydrogen - a sustainable energy carrier, Progress in Natural Science: Materials International 27 (1) (2017) 34–40, sI-HYDROGEN STORAGE MATERIALS.

[30] A. Züttel, Hydrogen storage methods, Naturwissenschaften 91 (4) (2004) 157–172.

[31] G. Kubilay Karayel, N. Javani, I. Dincer, A comprehensive assessment of energy storage options for green hydrogen, Energy Conversion and Management 291 (2023) 117311.

[32] J. E. Dec, Advanced compression-ignition engines—understanding the in-cylinder processes, Proceedings of the Combustion Institute 32 (2) (2009) 2727–2742.

[33] R. D. Reitz, G. Duraisamy, Review of high efficiency and clean reactivity controlled compression ignition (rcci) combustion in internal combustion engines, Progress in Energy and Combustion Science 46 (2015) 12–71.

[34] T. K. Sharma, G. A. P. Rao, K. M. Murthy, Homogeneous charge compression ignition (hcci) engines: A review, Archives of Computational Methods in Engineering 23 (4) (2016) 623–657.

[35] M. P. Musculus, P. C. Miles, L. M. Pickett, Conceptual models for partially premixed low-temperature diesel combustion, Progress in Energy and Combustion Science 39 (2) (2013) 246–283.

[36] C. Noehre, M. Andersson, B. Johansson, A. Hultqvist, Characterization of partially premixed combustion, in: Powertrain & Fluid Systems Conference and Exhibition, SAE International, 2006.

[37] S. K. Verma, S. Gaur, T. Akram, S. Gautam, A. Kumar, Emissions from homogeneous charge compression ignition (hcci) engine using different fuels: a review, Environmental Science and Pollution Research 29 (34) (2022) 50960–50969.

[38] M. Yao, Z. Zheng, H. Liu, Progress and recent trends in homogeneous charge compression ignition (hcci) engines, Progress in Energy and Combustion Science 35 (5) (2009) 398–437.

[39] G. Kalghatgi, L. Hildingsson, A. Harrison, B. Johansson, Autoignition quality of gasoline fuels in partially premixed combustion in diesel engines, Proceedings of the Combustion Institute 33 (2) (2011) 3015–3021.

[40] V. Manente, C.-G. Zander, B. Johansson, P. Tunestal, W. Cannella, An advanced internal combustion engine concept for low emissions and high efficiency from idle to max load using gasoline partially premixed combustion, in: SAE 2010 Powertrains Fuels Lubricants Meeting, SAE International, 2010.

[41] V. Manente, B. Johansson, P. Tunestal, Partially premixed combustion at high load using gasoline and ethanol, a comparison with diesel, in: SAE World Congress Exhibition, SAE International, 2009.

[42] V. Manente, B. Johansson, W. Cannella, Gasoline partially premixed combustion, the future of internal combustion engines?, International Journal of Engine Research 12 (3) (2011) 194–208.

[43] C. Li, P. Tunestal, M. Tuner, B. Johansson, Comparison of gasoline and primary reference fuel in the transition from hcci to ppc, in: International Powertrains, Fuels Lubricants Meeting, SAE International, 2017.

[44] M. Lundgren, J. Rosell, M. Richter, ⊠. Andersson, B. Johansson, A. Arne, M. Alden, Optical study on combustion transition from hcci to ppc with gasoline compression ignition in a hd engine, in: SAE 2016 World Congress and Exhibition, SAE International, 2016.

[45] V. Ravaglioli, F. Ponti, G. Silvagni, D. Moro, F. Stola, M. De Cesare, Performance assessment of gasoline ppc in a light-duty ci engine, in: WCX SAE World Congress Experience, SAE International, 2022.

[46] Quantification and Analysis of the Charge Cooling Effect of Methanol in a Compression Ignition Engine Utilizing PPC Strategy, Vol. Volume 1: Large Bore Engines; Fuels; Advanced Combustion of Internal Combustion Engine Division Fall Technical Conference.

[47] A. Matamis, S. Lonn, M. Tuner, O. Andersson, M. Richter, Optical characterization of methanol sprays and mixture formation in a compression-ignition heavy-duty engine, in: SAE Powertrains, Fuels Lubricants Meeting, SAE International, 2020.

[48] A. Matamis, S. Lonn, L. Luise, B. M. Vaglieco, M. Tuner, O. Andersson, M. Alden, M. Richter, Optical characterization of methanol compression-ignition combustion in a heavy-duty engine, Proceedings of the Combustion Institute 38 (4) (2021) 5509–5517.

[49] S. Shamun, C. Haşimoğlu, A. Murcak, Öivind Andersson, M. Tunér, P. Tunestål, Experimental investigation of methanol compression ignition in a high compression ratio hd engine using a box-behnken design, Fuel 209 (2017) 624–633.

[50] A. Garcia, A. Aziz, L. Xu, M. Tuner, Influence of injection timing on equivalence ratio stratification of methanol and isooctane in a heavy-duty compression ignition engine, in: SAE Powertrains, Fuels Lubricants Meeting, SAE International, 2020.

[51] M. Pucilowski, M. Jangi, S. Shamun, M. Tuner, X.-S. Bai, The effect of injection pressure on the nox emission rates in a heavy-duty dici engine running on methanol., in: International Powertrains, Fuels Lubricants Meeting, SAE International, 2017.

[52] C. White, R. Steeper, A. Lutz, The hydrogen-fueled internal combustion engine: a technical review, International Journal of Hydrogen Energy 31 (10) (2006) 1292–1305.

[53] H. Mathur, L. Das, Performance characteristics of a hydrogen fuelled s.i. engine using timed manifold injection, International Journal of Hydrogen Energy 16 (2) (1991) 115–127.

[54] T. Sandalcı, Y. Karagöz, Experimental investigation of the combustion characteristics, emissions and performance of hydrogen port fuel injection in a diesel engine, International Journal of Hydrogen Energy 39 (32) (2014) 18480–18489.

[55] S. Verhelst, Recent progress in the use of hydrogen as a fuel for internal combustion engines, International Journal of Hydrogen Energy 39 (2) (2014) 1071–1085.

[56] N. Kawahara, E. Tomita, Visualization of auto-ignition and pressure wave during knocking in a hydrogen spark-ignition engine, International Journal of Hydrogen Energy 34 (7) (2009) 3156–3163.

[57] A. Mohammadi, M. Shioji, Y. Nakai, W. Ishikura, E. Tabo, Performance and combustion characteristics of a direct injection si hydrogen engine, International Journal of Hydrogen Energy 32 (2) (2007) 296–304.

[58] C. Donaldson, Dup., and snedeker rs, a study of free jet impingement. part 1. mean properties of free and impinging jets, J. Fluid Mech 45 (2) (1971) 281–319.

[59] A. Hamzehloo, P. Aleiferis, Large eddy simulation of highly turbulent underexpanded hydrogen and methane jets for gaseous-fuelled internal combustion engines, International Journal of Hydrogen Energy 39 (36) (2014) 21275–21296.

[60] A. Hamzehloo, P. G. Aleiferis, Les and rans modelling of under-expanded jets with application to gaseous fuel direct injection for advanced propulsion systems, International Journal of Heat and Fluid Flow 76 (2019) 309–334.

[61] A. Dauptain, B. Cuenot, L. Y. M. Gicquel, Large eddy simulation of stable supersonic jet impinging on flat plate, AIAA Journal 48 (10) (2010) 2325–2338.

[62] V. Vuorinen, J. Yu, S. Tirunagari, O. Kaario, M. Larmi, C. Duwig, B. J. Boersma, Large-eddy simulation of highly underexpanded transient gas jets, Physics of Fluids 25 (1) (2013) 016101.

[63] M. Banholzer, W. Vera-Tudela, C. Traxinger, M. Pfitzner, Y. Wright, K. Boulouchos, Numerical investigation of the flow characteristics of underexpanded methane jets, Physics of Fluids 31 (5) (2019) 056105.

[64] C. M. White, S. Kaiser, Piv and plif to evaluate mixture formation in a direct-injection hydrogen-fuelled engine, SAE International Journal of Engines 1 (1) (2008) 657–668.

[65] X. Yang, X. Wang, Q. Dong, Z. Ni, J. Song, T. Zhou, Experimental study on the two-phase fuel transient injection characteristics of the high-pressure natural gas and diesel co-direct injection engine, Energy 243 (2022) 123114.

[66] T. Kamimoto, T. Kohama, H. Seki, Y. Yamamoto, Y. Moriyoshi, Development of a transient hydrogen jet in a high-swirl constant volume chamber, in: J. H. Whitelaw, F. Payri, C. Arcoumanis, J. M. Desantes (Eds.), Thermo- and Fluid

Dynamic Processes in Diesel Engines 2, Springer Berlin Heidelberg, Berlin, Heidelberg, 2004, pp. 49–60.

[67] P. Ouellette, Direct injection of natural gas for diesel engine fueling, Ph.D. thesis, University of British Columbia (1996).

[68] J. S. Turner, The 'starting plume' in neutral surroundings, Journal of Fluid Mechanics 13 (3) (1962) 356–368.

[69] H. Rottengruber, M. Berckmüller, G. Elsässer, N. Brehm, C. Schwarz, Direct-injection hydrogen si-engine - operation strategy and power density potentials, in: 2004 Powertrain Fluid Systems Conference Exhibition, SAE International, 2004.

[70] Y. Li, W. Gao, P. Zhang, Y. Ye, Z. Wei, Effects study of injection strategies on hydrogen-air formation and performance of hydrogen direct injection internal combustion engine, International Journal of Hydrogen Energy 44 (47) (2019) 26000–26011.

[71] Y. Takagi, M. Oikawa, R. Sato, Y. Kojiya, Y. Mihara, Near-zero emissions with high thermal efficiency realized by optimizing jet plume location relative to combustion chamber wall, jet geometry and injection timing in a direct-injection hydrogen engine, International Journal of Hydrogen Energy 44 (18) (2019) 9456–9465.

[72] T. Wallner, A. M. Nande, J. Naber, Evaluation of injector location and nozzle design in a direct-injection hydrogen research engine, in: 2008 SAE International Powertrains, Fuels and Lubricants Congress, SAE International, 2008.

[73] T. Wallner, N. S. Matthias, R. Scarcelli, Influence of injection strategy in a high-efficiency hydrogen direct injection engine, SAE International Journal of Fuels and Lubricants 5 (1) (2011) 289–300.

[74] R. Scarcelli, T. Wallner, N. Matthias, V. Salazar, S. Kaiser, Numerical and optical evolution of gaseous jets in direct injection hydrogen engines, in: SAE 2011 World Congress Exhibition, SAE International, 2011.

[75] V. M. Salazar, S. A. Kaiser, An optical study of mixture preparation in a hydrogen-fueled engine with direct injection using different nozzle designs, SAE International Journal of Engines 2 (2) (2009) 119–131.

[76] M. K. Roy, N. Kawahara, E. Tomita, T. Fujitani, High-pressure hydrogen jet and combustion characteristics in a direct-injection hydrogen engine, SAE International Journal of Fuels and Lubricants 5 (3) (2012) 1414–1425.

[77] B. Petersen, J. Ghandhi, Transient high-pressure hydrogen jet measurements, SAE Transactions 115 (2006) 354–364.

[78] Y. Lei, Y. Wu, T. Qiu, D. Zhou, X. Lian, W. Jin, Experimental study of dual-fuel diesel/natural gas high-pressure injection, ACS Omega 8 (1) (2023) 519–528.

[79] T. R. White, Simultaneous diesel and natural gas injection for dual-fuelling compression-ignition engines, Thesis, University of New South Wales, Sydney (2006).

[80] K. Pan, J. Wallace, Computational studies of fuel injection strategies on natural gas combustion characteristics in direct-injection engines, Fuel 288 (2021) 119823.

[81] G. Fink, M. Jud, T. Sattelmayer, Influence of the Spatial and Temporal Interaction Between Diesel Pilot and Directly Injected Natural Gas Jet on Ignition and Combustion Characteristics, Journal of Engineering for Gas Turbines and Power 140 (10) (2018) 102811.

[82] G. Fink, M. Jud, T. Sattelmayer, Fundamental Study of Diesel-Piloted Natural Gas Direct Injection Under Different Operating Conditions, Journal of Engineering for Gas Turbines and Power 141 (9) (2019) 091006.

[83] X. Yang, V. Bonfochi Vinhaes, M. Turcios, G. McTaggart-Cowan, J. Huang, J. Naber, M. Shahbakhti, H. Schmidt, W. Atkinson, Process for study of micro-pilot diesel-ng dual fuel combustion in a constant volume combustion vessel utilizing the premixed pre-burn procedure, in: WCX SAE World Congress Experience, SAE International, 2019.

[84] M. Li, G. Liu, X. Liu, Z. Li, Q. Zhang, B. Shen, Performance of a direct-injection natural gas engine with multiple injection strategies, Energy 189 (2019) 116363.

[85] P. Rorimpandey, H. L. Yip, A. Srna, G. Zhai, A. Wehrfritz, S. Kook, E. R. Hawkes, Q. N. Chan, Hydrogen-diesel dual-fuel direct-injection (h2ddi) combustion under compression-ignition engine conditions, International Journal of Hydrogen Energy 48 (2) (2023) 766–783.

[86] P. Rorimpandey, G. Zhai, S. Kook, E. R. Hawkes, Q. N. Chan, Effects of energy-share and ambient oxygen concentration on hydrogen-diesel dual-fuel direct-injection (h2ddi) combustion in compression-ignition conditions, International Journal of Hydrogen Energy 49 (2024) 1346–1361.

[87] X. Liu, A. Srna, H. L. Yip, S. Kook, Q. N. Chan, E. R. Hawkes, Performance and emissions of hydrogen-diesel dual direct injection (h2ddi) in a single-cylinder compression-ignition engine, International Journal of Hydrogen Energy 46 (1) (2021) 1302–1314.

[88] X. Liu, G. Seberry, S. Kook, Q. N. Chan, E. R. Hawkes, Direct injection of hydrogen main fuel and diesel pilot fuel in a retrofitted single-cylinder compression ignition engine, International Journal of Hydrogen Energy 47 (84) (2022) 35864–35876.

[89] C. Ramsay, K. R. Dinesh, Numerical modelling of a heavy-duty diesel-hydrogen dual-fuel engine with late high pressure hydrogen direct injection and diesel pilot, International Journal of Hydrogen Energy 49 (2024) 674–696.

[90] A. Hadadpour, M. Jangi, X. S. Bai, The effect of splitting timing on mixing in a jet with double injections, Flow, Turbulence and Combustion 101 (4) (2018) 1157–1171.

[91] A. Hadadpour, M. Jangi, K. M. Pang, X. Song Bai, The role of a split injection strategy in the mixture formation and combustion of diesel spray: A large-eddy simulation, Proceedings of the Combustion Institute 37 (4) (2019) 4709–4716.

[92] P. G. Aleiferis, M. F. Rosati, Controlled autoignition of hydrogen in a direct-injection optical engine, Combustion and Flame 159 (7) (2012) 2500–2515.

[93] O. Stenlåås, M. Christensen, R. Egnell, B. Johansson, F. Mauss, Hydrogen as homogeneous charge compression ignition engine fuel, SAE Transactions 113 (2004) 1317–1326.

[94] J. Gomes Antunes, R. Mikalsen, A. Roskilly, An experimental study of a direct injection compression ignition hydrogen engine, International Journal of Hydrogen Energy 34 (15) (2009) 6516–6522.

[95] T. Shudo, S. Oba, Mixture distribution measurement using laser induced breakdown spectroscopy in hydrogen direct injection stratified charge, International Journal of Hydrogen Energy 34 (5) (2009) 2488–2493.

[96] J. Naber, D. Siebers, Hydrogen combustion under diesel engine conditions, International Journal of Hydrogen Energy 23 (5) (1998) 363–371.

[97] T. Tsujimura, S. Mikami, N. Achiha, Y. Tokunaga, J. Senda, H. Fujimoto, A study of direct injection diesel engine fueled with hydrogen, SAE Transactions 112 (2003) 390–405.

[98] H. L. Yip, A. Srna, X. Liu, S. Kook, E. R. Hawkes, Q. N. Chan, Visualization of hydrogen jet evolution and combustion under simulated direct-injection compression-ignition engine conditions, International Journal of Hydrogen Energy 45 (56) (2020) 32562–32578.

[99] H. L. Yip, A. Srna, A. Wehrfritz, S. Kook, E. R. Hawkes, Q. N. Chan, A parametric study of autoigniting hydrogen jets under compression-ignition engine conditions, International Journal of Hydrogen Energy 47 (49) (2022) 21307–21322.

[100] R. Babayev, A. Andersson, A. S. Dalmau, H. G. Im, B. Johansson, Computational characterization of hydrogen direct injection and nonpremixed combustion in a compression-ignition engine, International Journal of Hydrogen Energy 46 (35) (2021) 18678–18696.

[101] R. Babayev, A. Andersson, A. Serra Dalmau, H. G. Im, B. Johansson, Computational comparison of the conventional diesel and hydrogen direct-injection compression-ignition combustion engines, Fuel 307 (2022) 121909.

[102] X. Liu, H. Aljabri, N. Panthi, A. S. AlRamadan, E. Cenker, A. T. Alshammari, G. Magnotti, H. G. Im, Computational study of hydrogen engine combustion strategies: Dual-fuel compression ignition with port- and direct-injection, prechamber combustion, and spark-ignition, Fuel 350 (2023) 128801.

[103] A. Aziz, L. Xu, A. Garcia, M. Tuner, Influence of injection timing on equivalence ratio stratification of methanol and isooctane in a heavy-duty compression ignition engine, SAE 2020-01-2069, 2020 (2020).

[104] A. Leonard, Energy cascade in large-eddy simulations of turbulent fluid flows, in: F. Frenkiel, R. Munn (Eds.), Turbulent Diffusion in Environmental Pollution, Vol. 18 of Advances in Geophysics, Elsevier, 1975, pp. 237–248.

[105] F. G. Schmitt, About Boussinesq's turbulent viscosity hypothesis: historical remarks and a direct evaluation of its validity, Comptes Rendus Mécanique 335 (9-10) (2007) 617–627.

[106] P. K. Senecal, E. Pomraning, K. J. Richards, T. E. Briggs, C. Y. Choi, R. M. McDavid, M. A. Patterson, Multi-dimensional modeling of direct-injection diesel spray liquid length and flame lift-off length using cfd and parallel detailed chemistry, SAE Transactions 112 (2003) 1331–1351.

[107] S. Turns, An Introduction to Combustion: Concepts and Applications, McGraw-Hill series in mechanical engineering, McGraw-Hill, 2000.

[108] J. Chomiak, Combustion a study in theory, fact and application (1 1990). URL https://www.osti.gov/biblio/5894595

[109] R. Reitz, Modeling atomization processes in high-pressure vaporizing sprays, Atomisation Spray Technology 3 (1987) 309–337.

[110] J. C. Beale, R. D. Reitz, Modeling spray atomization with the kelvin-helmholtz/rayleigh-taylor hybrid model, Atomization spray 9 (6) (1999).

[111] K. J. Richards, P. K. Senecal, E. Pomraning, Converge 3.0, Convergent Science, Madison, WI (2021).

[112] J. B. Heywood, Internal combustion engine fundamentals, Mcgraw-hill New York, 1988.

[113] L. Xu, X.-S. Bai, M. Jia, Y. Qian, X. Qiao, X. Lu, Experimental and modeling study of liquid fuel injection and combustion in diesel engines with a common rail injection system, Applied Energy 230 (2018) 287–304.

[114] X. Liu, H. Wang, L. Wei, J. Liu, R. D. Reitz, M. Yao, Development of a reduced toluene reference fuel (trf)-2,5-dimethylfuran-polycyclic aromatic hydrocarbon (pah) mechanism for engine applications, Combustion and Flame 165 (2016) 453–465.

[115] T. Lucchini, G. D'Errico, H. Jasak, Z. Tukovic, Automatic mesh motion with topological changes for engine simulation, SAE 2007-01-0170 (2007).

[116] X. Yang, Q. Dong, X. Wang, T. Zhou, D. Wei, An experimental study on the needle valve motion characteristics of high pressure natural gas and diesel co-direct injector, Energy 265 (2023) 126257.

[117] T. Yao, Y. Pei, B.-J. Zhong, S. Som, T. Lu, K. H. Luo, A compact skeletal mechanism for n-dodecane with optimized semi-global low-temperature chemistry for diesel engine simulations, Fuel 191 (2017) 339–349.

[118] E. Ranzi, C. Cavallotti, A. Cuoci, A. Frassoldati, M. Pelucchi, T. Faravelli, New reaction classes in the kinetic modeling of low temperature oxidation of n-alkanes, Combustion and Flame 162 (5) (2015) 1679–1691.

[119] L. Seidel, K. Moshammer, X. Wang, T. Zeuch, K. Kohse-Höinghaus, F. Mauss, Comprehensive kinetic modeling and experimental study of a fuel-rich, premixed n-heptane flame, Combustion and Flame 162 (5) (2015) 2045–2058.

[120] N. Peters, F. A. Williams, Liftoff characteristics of turbulent jet diffusion flames, AIAA Journal 21 (1983) 423–429.

[121] T. Gautam, Lift-off heights and visible lengths of vertical turbulent jet diffusion flames in still air, Combustion Science and Technology 41 (1-2) (1984) 17–29.

[122] C. Gong, M. Jangi, X.-S. Bai, Large eddy simulation of n-dodecane spray combustion in a high pressure combustion vessel, Applied Energy 136 (2014) 373–381.

[123] L. Pickett, D. Siebers, C. A. Idicheria, Relationship between ignition processes and the lift-off length of diesel fuel jets, in: SAE 2005 World Congress & Exhibition, SAE International, 2005.

Scientific publications

Author contributions

Paper I: Comparison of efficiency and emission characteristics in a direct-injection compression ignition engine fuelled with iso-octane and methanol under low temperature combustion conditions

Applied Energy, 2022, 312, 118714
Leilei Xu, **Mark Treacy**, Yan Zhang, Amir Aziz, Martin Tuner, Xue-Song Bai

This paper numerically investigates methanol and iso-octane in low-temperature combustion by sweeping the SOI from the HCCI to late PPC range. The simulated cases are based on and validated against engine experiments. This work shows that methanol achieves a more fuel-lean mixture compared to iso-octane, which is more stratified. The performance and emissions of both fuels are analysed and discussed across all SOIs.

The candidate supported the data analysis of the numerical simulations and contributed to writing the manuscript.

Paper II: Performance of a methanol fuelled direct-injection compression ignition heavy-duty engine under low temperature combustion conditions

12th Mediterranean Combustion Symposium, 2023, Luxor, Egypt
Mark Treacy, Leilei Xu, Hesameddin Fatehi, Xue-Song Bai

This paper focuses on methanol low-temperature combustion in a heavy-duty engine. Numerical simulations are carried out on an SOI sweep covering HCCI, tran-

sition to PPC and the PPC range. The in-cylinder combustion processes are discussed leading to a better understanding of the performance and emissions.

The candidate carried out data analysis on the numerical simulations and wrote the manuscript with advice from the co-authors.

Paper III: Performance and emissions of a novel high-pressure direct injection dual-fuel engine

Under review in Fuel
Mark Treacy, Ahmad Hadadpour, Xue-Song Bai, Hesameddin Fatehi

This work uses numerical simulations to investigate diesel-hydrogen dual-fuel strategies in a compression ignition engine. The simulations were validated against engine experiments. The SOI and rail pressure of both fuels was investigated. The early injection timings provided the highest efficiency due to the lower exhaust losses that were observed to be a key contributor to the lower efficiency in the late injection cases. A relationship between NO_x and efficiency trends was observed.

The candidate performed all the numerical simulations. The candidate wrote the manuscript with supervision by Xue-Song Bai and Hesameddin Fatehi and advice from Ahmad Hadadpour.

Paper IV: A Computational Fluid Dynamics Study of Advanced Injection Strategies for Compression Ignition Hydrogen Engines

Manuscript to be submitted
Mark Treacy, Ahmad Hadadpour, Xue-Song Bai, Hesameddin Fatehi

Using a numerical case set-up from the duel-fuel simulations, the HYZERO concept was investigated. For these cases, the carbon is entirely removed from the system and the total injected hydrogen mass is divided into a pilot and main injection. A complex relationship between dwell time and pilot energy share was observed. The relationship must be managed in order to achieve a combustible fuel-air mixture from the pilot injection to avoid misfire or uncontrolled combustion. To achieve controlled combustion, the intake temperature was increased from the baseline case. Various pilot energy shares and dwell time were investigated to identify the operating window. Additionally, the SOI was shifted towards TDC to achieve controlled combustion using the baseline intake temperature.

The candidate performed all the numerical simulations. The candidate wrote the manuscript with supervision by Xue-Song Bai and Hesameddin Fatehi and advice from Ahmad Hadadpour.

Paper V: Large eddy simulation of diesel-hydrogen dual-fuel flames

Manuscript to be submitted
Mark Treacy, Xue-Song Bai, Hesameddin Fatehi

This work uses LES to investigate diesel-hydrogen dual-fuel combustion in a constant volume. The simulations are based on experiments available in literature. In this work, three cases are investigated where the dwell time is investigated. For each of the cases, the interaction between the hydrogen and n-heptane sprays is investigated as well as the combustion behavior of the hydrogen jet.

The candidate performed all the numerical simulations. The candidate wrote the manuscript with the supervision of Xue-Song Bai and Hesameddin Fatehi.